Magnetic Reconnection in Plasma
Stockholm, Sweden, August 10 – 14, 2015

Instabilities and Magnetic Reconnection Near the Heliopause

N.V. Pogorelov[1,2]

[1]University of Alabama in Huntsville, Department of Space Science
[2]Center for Space Plasma and Aeronomic Research

Outline

1. **Magnetic field and charge exchange effects.**
2. **Transition to turbulence in the inner heliosheath.**
3. **Mixing of the SW and LISM plasmas the heliopause.**
4. **Heliotail and TeV cosmic ray anisotropy.**

Properties of the solar wind and the local interstellar medium

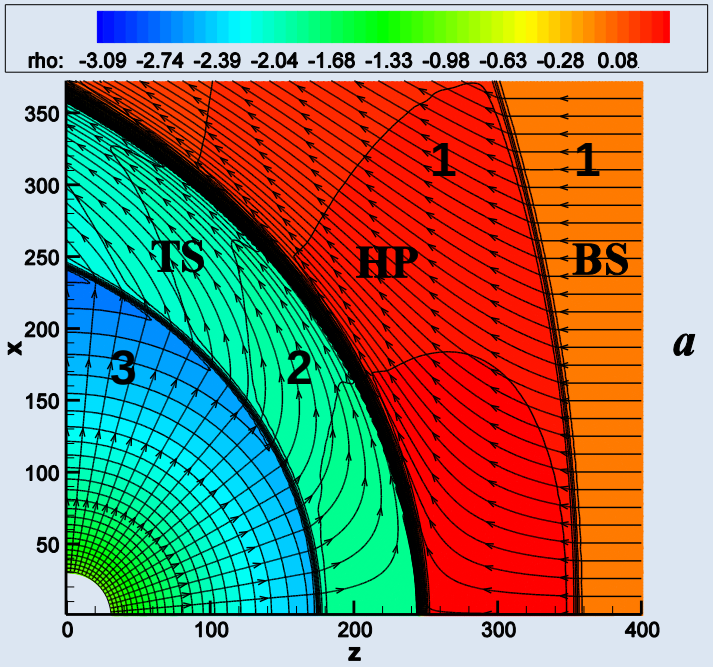

a

Solar wind:

V_p = 450 km/s, n_p = 7.4 cm^{-3}, and T_p = 51100 K.

LISM:

V_∞ = 26.4 km/s, n_∞=0.05 – 0.07 cm^{-3}, T_∞ = 6500 K, $n_{H\infty}$ = 0.15 – 0.18 cm^{-3}.

Neutral particles play a major role in the SW-LISM interaction (Wallis 1971, 1975; Baranov & Malama 1993; Zank et al., 1996; Fahr et al. 2000; Florinski et al. 2003; Izmodenov et al., ***2005; Heerikhuisen et al., 2006, 2007).***

The solar wind (SW) termination shock weakens due to the SW deceleration and heating; interstellar hydrogen atoms are filtrated at the heliopause due to their intensified charge exchange with decelerated ions; the LISM velocity and temperature change due to the LISM charge exchange with the hot secondary H atoms originating in the compressed solar wind behind the termination shock.

The system of MHD equations in the symmetrizable Godunov's form with the charge-exchange/collisional terms

$$\frac{\partial}{\partial t}\begin{bmatrix}\rho\\ \rho\mathbf{v}\\ e\\ \mathbf{B}\end{bmatrix} + \nabla\cdot\begin{bmatrix}\rho\mathbf{v}\\ \rho\mathbf{v}\mathbf{v} + p_0\hat{\mathbf{I}} - \dfrac{\mathbf{B}\mathbf{B}}{4\pi}\\ (e+p_0)\,\mathbf{v} - \dfrac{\mathbf{B}(\mathbf{v}\cdot\mathbf{B})}{4\pi}\\ \mathbf{v}\mathbf{B} - \mathbf{B}\mathbf{v}\end{bmatrix} = -\begin{bmatrix}0\\ \dfrac{\mathbf{B}}{4\pi}\\ \dfrac{\mathbf{v}\cdot\mathbf{B}}{4\pi}\\ \mathbf{v}\end{bmatrix}\times\nabla\cdot\mathbf{B} + \begin{bmatrix}0\\ \mathbf{H}^{\mathrm{m}}_{\mathrm{p-H}}\\ H^{\mathrm{e}}_{\mathrm{p-H}}\\ 0\end{bmatrix}.$$

Collisional terms are derived from the kinetic transport equations for the protons and neutral species, and we use either pitch-angle averaged or differential cross-sections for corresponding processes. For example, using stochastic Monte Carlo simulations (Baranov & Malama 1993; Izmodenov et al. 2005; Heerikhuisen et al. 2006, 2007).

Three-dimensional structure of the heliosphere in the presence of the IMF and ISMF

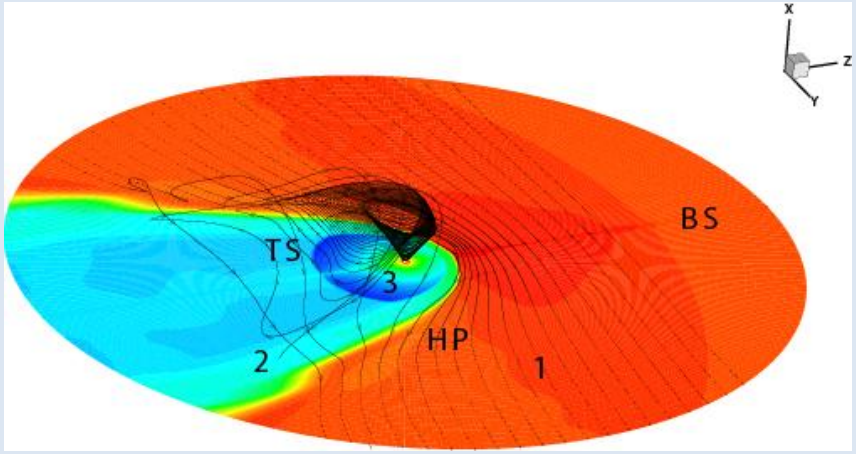

ISMF draping around the HP and an IMF spiral: ISMF is perpendicular to the LISM velocity vector and parallel to the ecliptic plane

From Pogorelov, Zank & Ogino (2004)

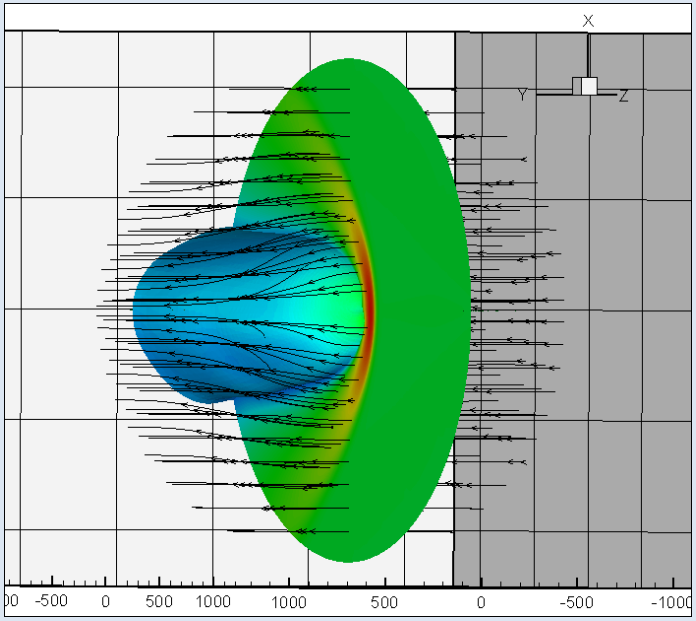

Magnetic pressure exerted perpendicular to the magnetic field direction compresses the heliopause in the north-south direction

ISMF perpendicular to the LISM velocity and tilted 60° to the ecliptic plane

Cross-sections of the widest and narrowest flaring of the heliopause

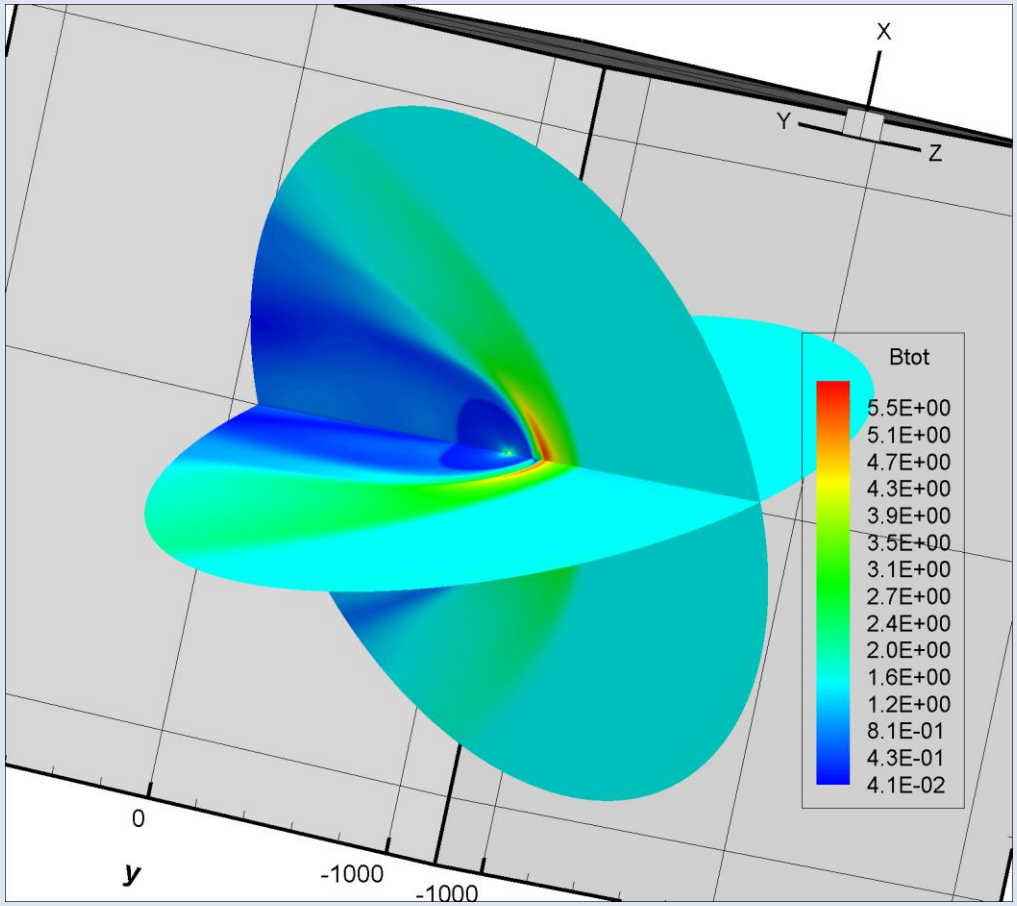

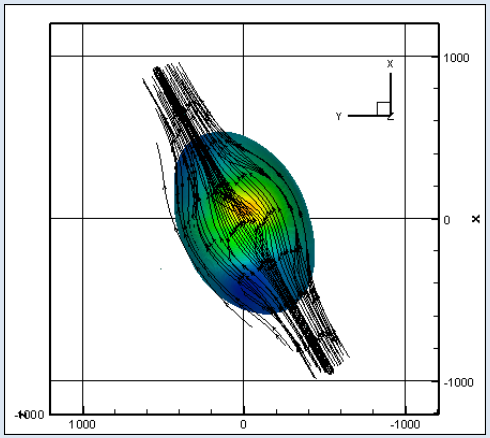

The HP rotates under the action of magnetic pressure and aligns with the *BV*-plane (the plane formed by B_∞ and V_∞

Initially planar HCS bends and rotates with respect to the z-axis, which is parallel to V_∞.

From Pogorelov, Zank & Ogino (2004)

The angle between the ISMF and the LISM velocity is 45° and B_∞= 2.5 μG (BV-plane coincides with the meridional plane). North-south asymmetries of the TS and HP.

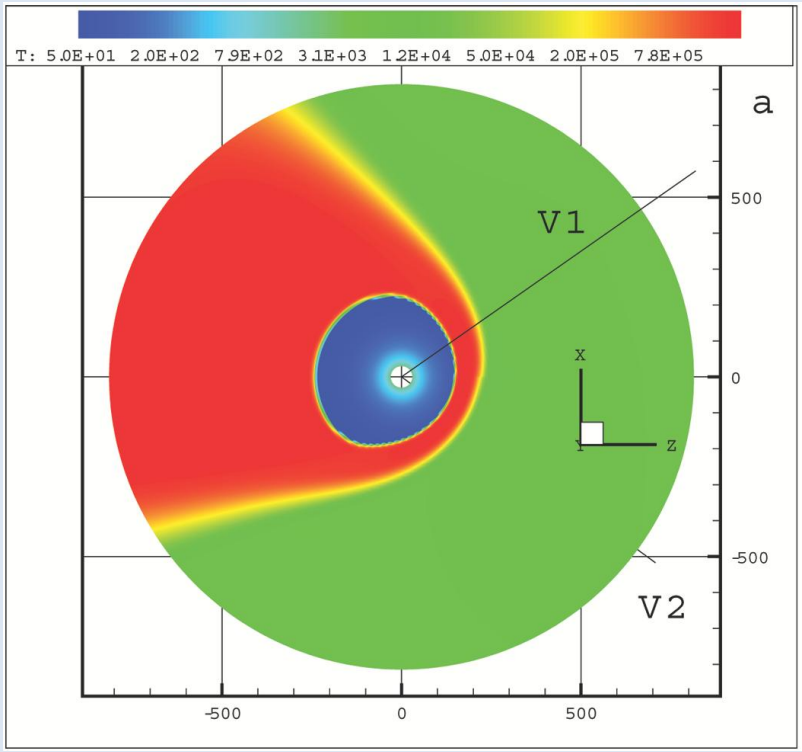

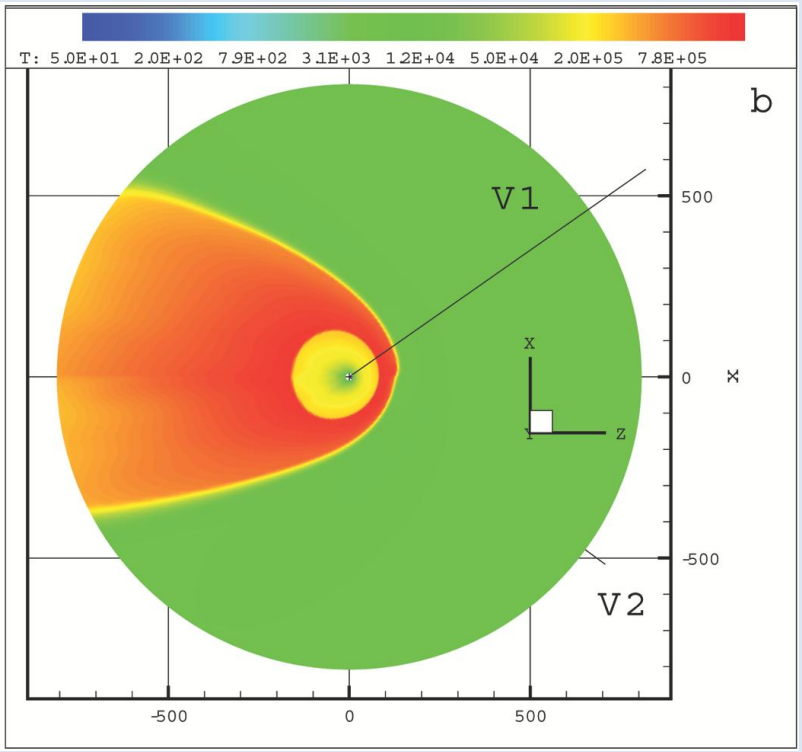

No neutrals, no IMF

With IMF and $n_{H\infty}$ = 0.15 cm^{-3}

Asymmetry of discontinuities with respect to the ecliptic plane becomes substantially less pronounced! V1-V2 asymmetry: 11 AU without neutrals and 2 AU with charge exchange. Neutral H density increase further symmetrizes the heliosheath.

Plasma density distribution in the *V1-V2* plane for the ISMF strength 3 μG (left) and 4 μG (right)

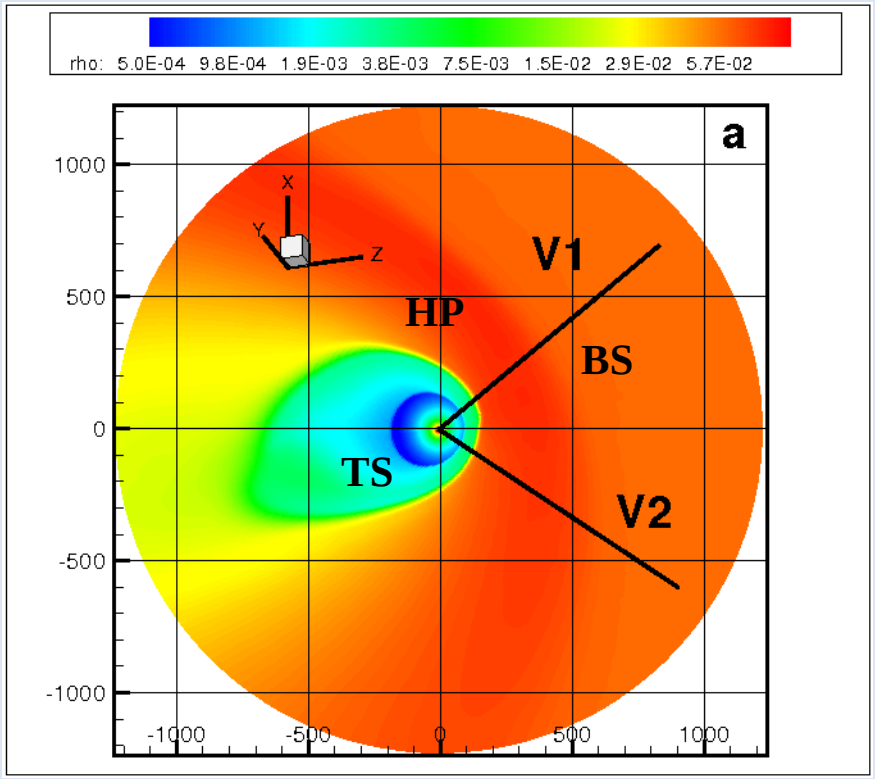

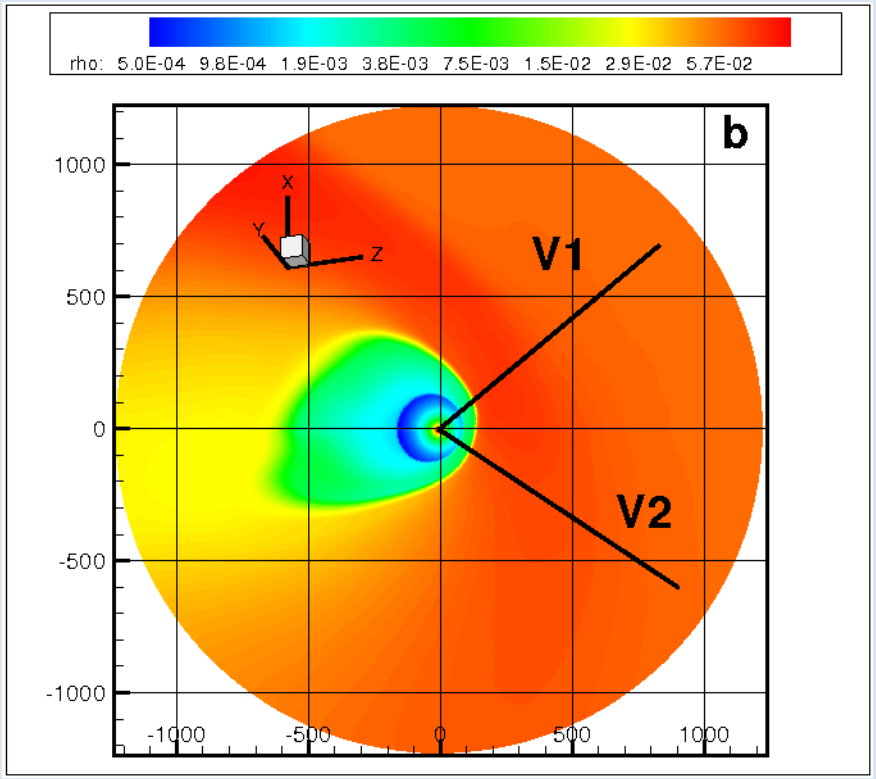

The TS heliocentric distance in the V2 direction is ~4 AU smaller than in the V1 direction in the former case and 9.5 AU smaller in the latter case.

The heliopause colored by the sign of B_R, the hydrogen deflection plane, the Galactic plane, and the trajectories of the V1 and V2 spacecraft

Pogorelov, Heerikhuisen, Zank (2008)

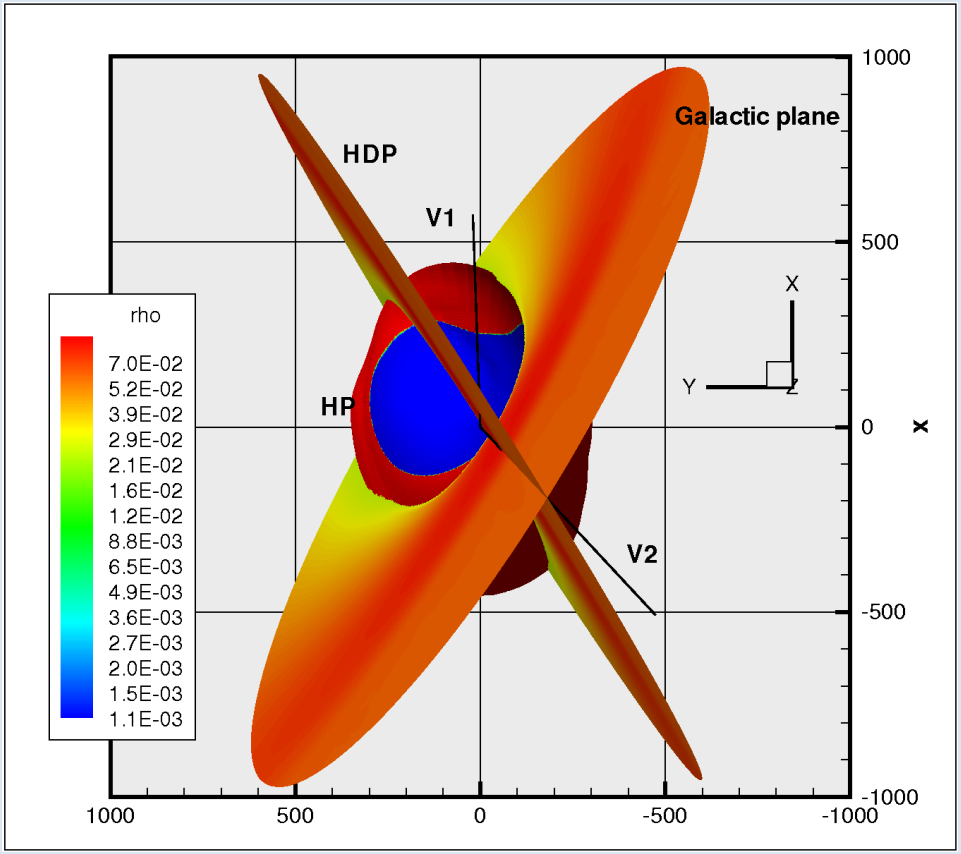

The HP is not symmetric with respect to the BV-plane!

H-atom deflection almost entirely in the BV-plane!

***BV*-plane parallel to the HDP, B_∞ at 30° to V_∞ (B_∞ = 3 μG), $n_{H\infty}$ = 0.15 cm^{-3}**

The LISM parameters are chosen to fit the IBEX ribbon data.

Magnetic filed intensity measured by ACE at 1 AU

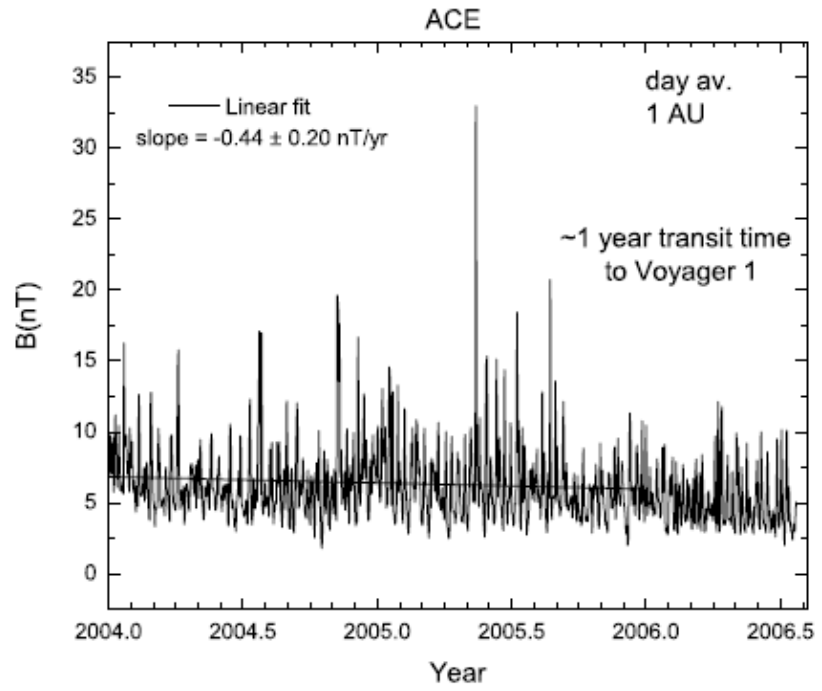

FIG. 2.—*ACE* observations of daily averages of the magnetic field strength *B* from 2004.0 to 2006.5. The straight line in the figure, a linear least-squares fit to the data from 2005.0 to 2006.0, has a negative slope, in contrast to the increase in *B* observed by *V1* during the corresponding interval displaced ~1 year later.

From Burlaga, Ness, and Acuña (2007)

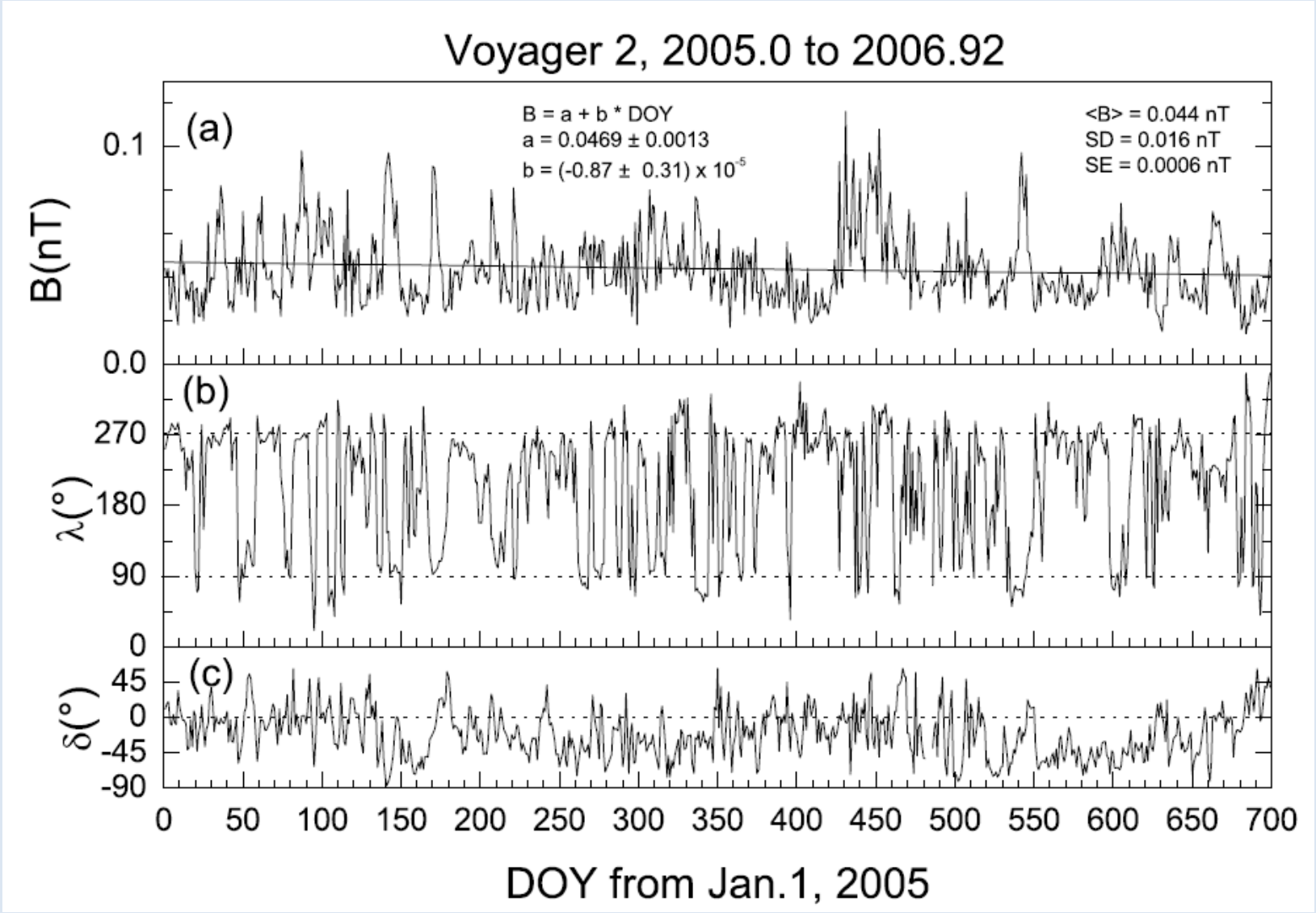

From Burlaga, Ness, and Acuña (2007)

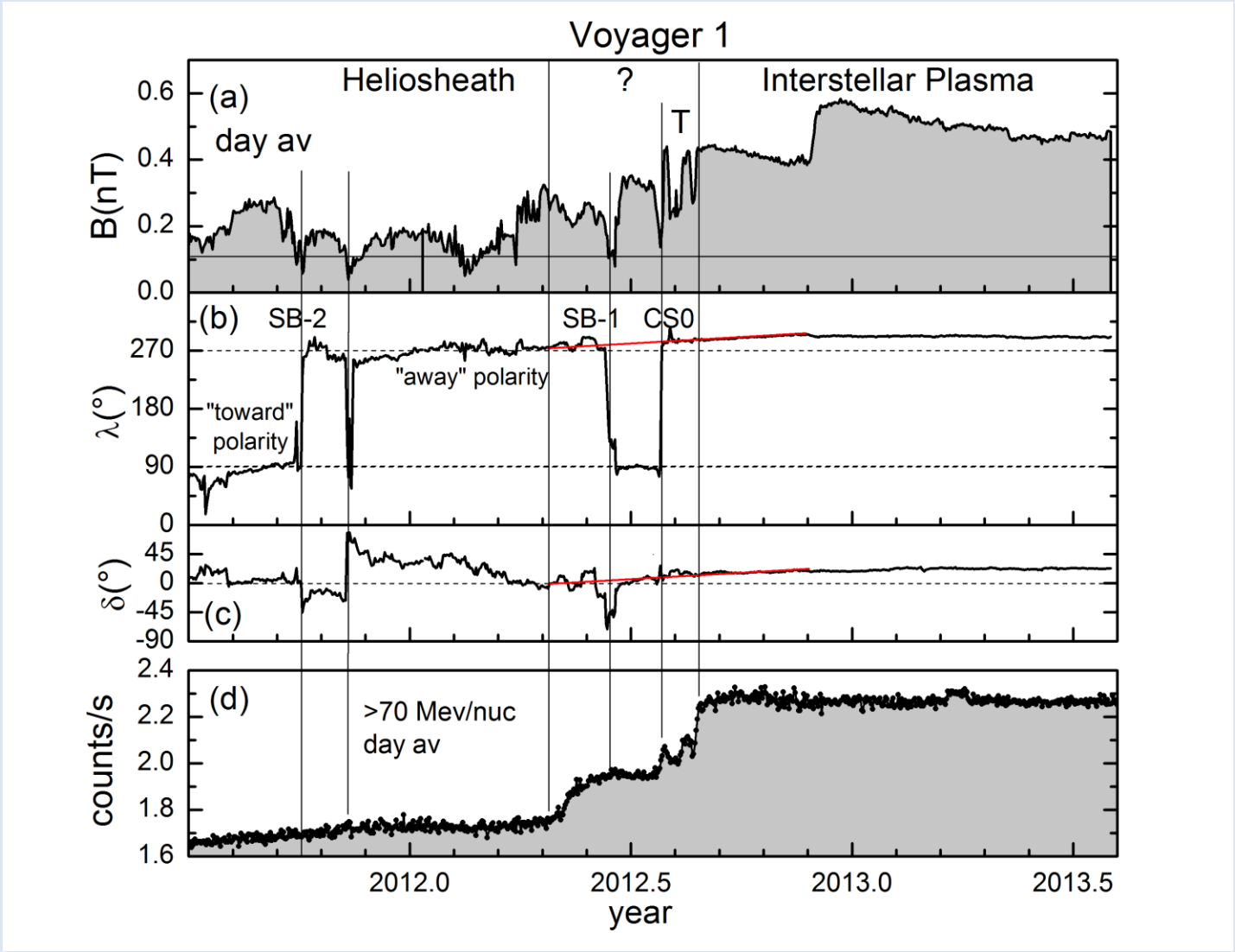

From Burlaga & Ness (2014)

Heliospheric current sheet / sectors in the heliosheath

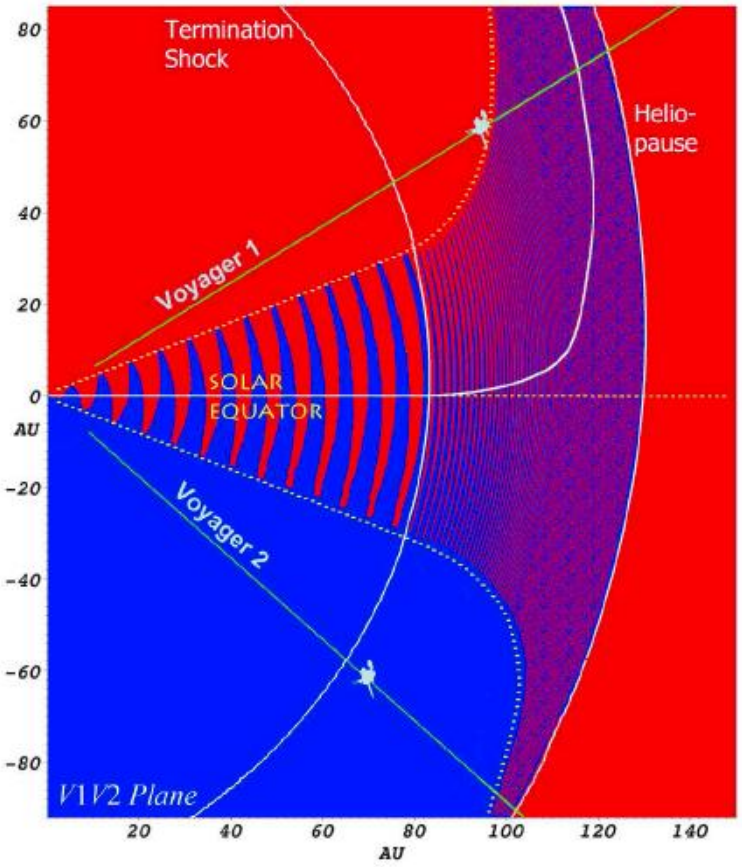

Figure 5: The HCS shape in the plane formed by the V1 and V2 trajectories.

2 different approaches are pursued:

(1) keep the dipolar field as is and let it dissipate due to turbulence near the heliopause;

(2) assume a unipolar field and assign the signs afterwards.

Unipolar HMF simulation of Borovikov et al. (2011).
Similar approaches were used by Czechowski et al., Izmodenov et al., and Florinski et al.

Transition to chaotic behavior in the IHS (parameters from Opher et al., 2012)

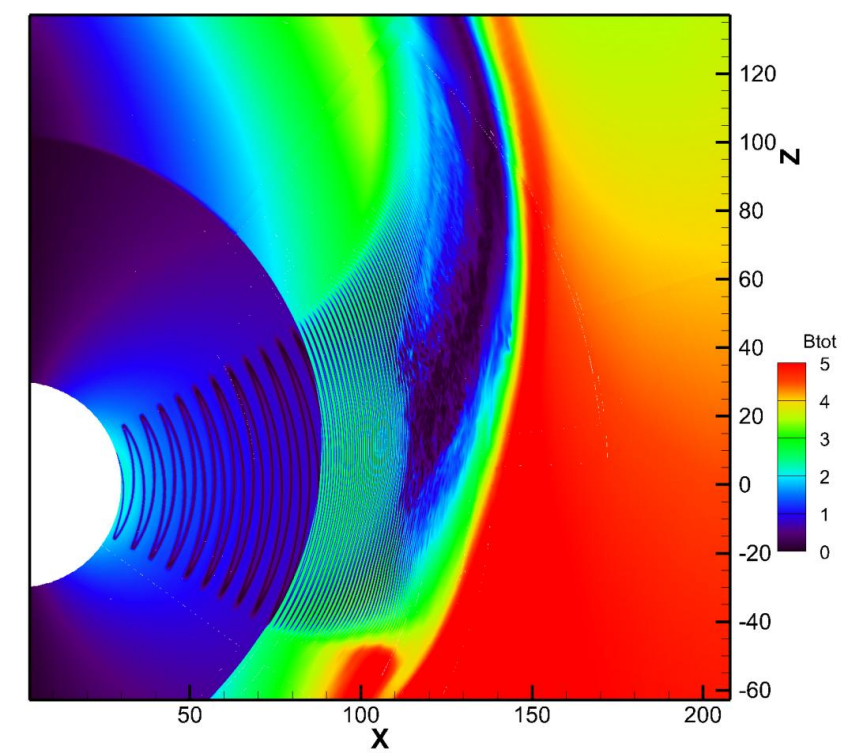

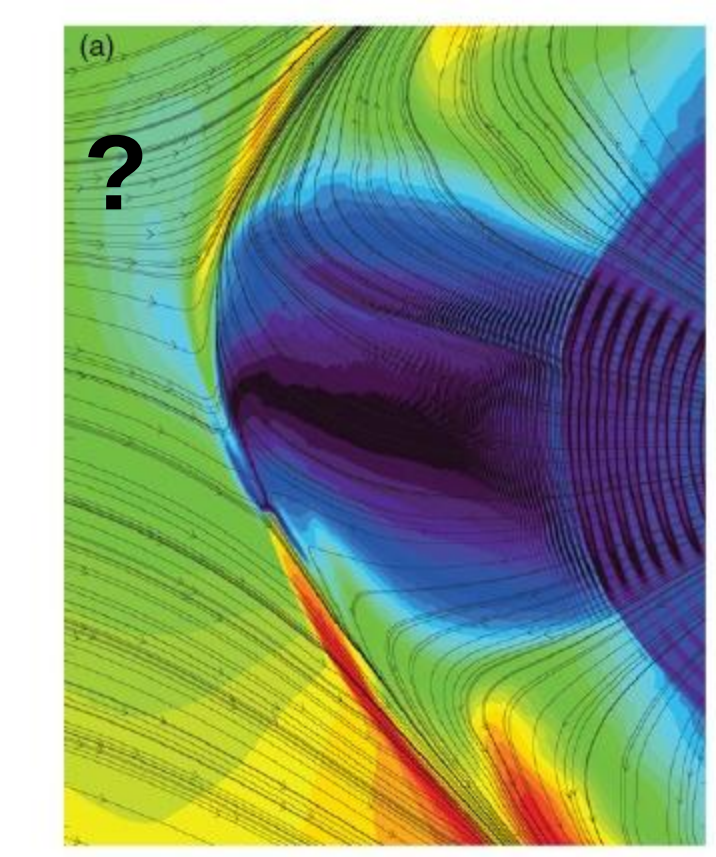

The distribution of |B| using the same color scale: no irregular structures or tangential discontinuities disrupting the heliospheric current sheet are observed

Transition to chaotic behavior in the IHS (Pogorelov et al., 2013)

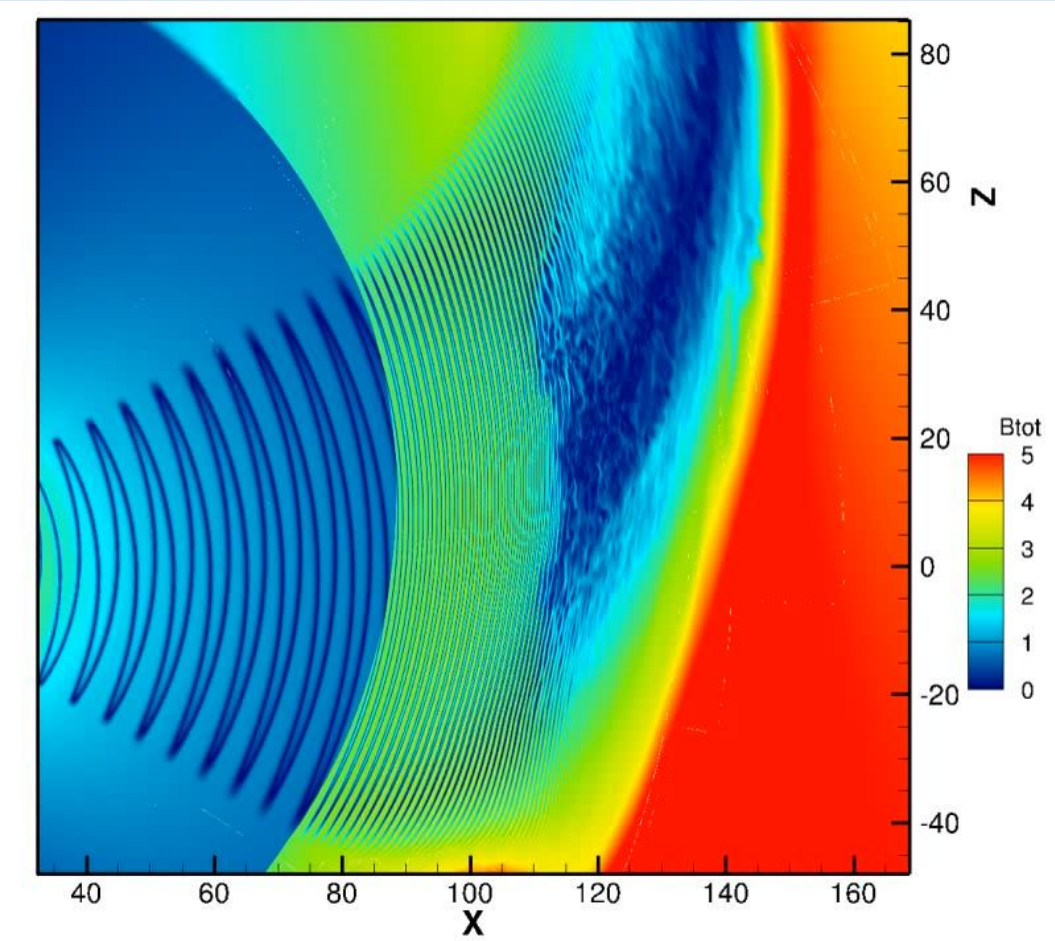

Evolution of the heliospheric magnetic filed in the inner heliosheath: the reason is tearing-mode instability due to numerical dissipation. In reality, such turbulization should occur closer to the heliopause.

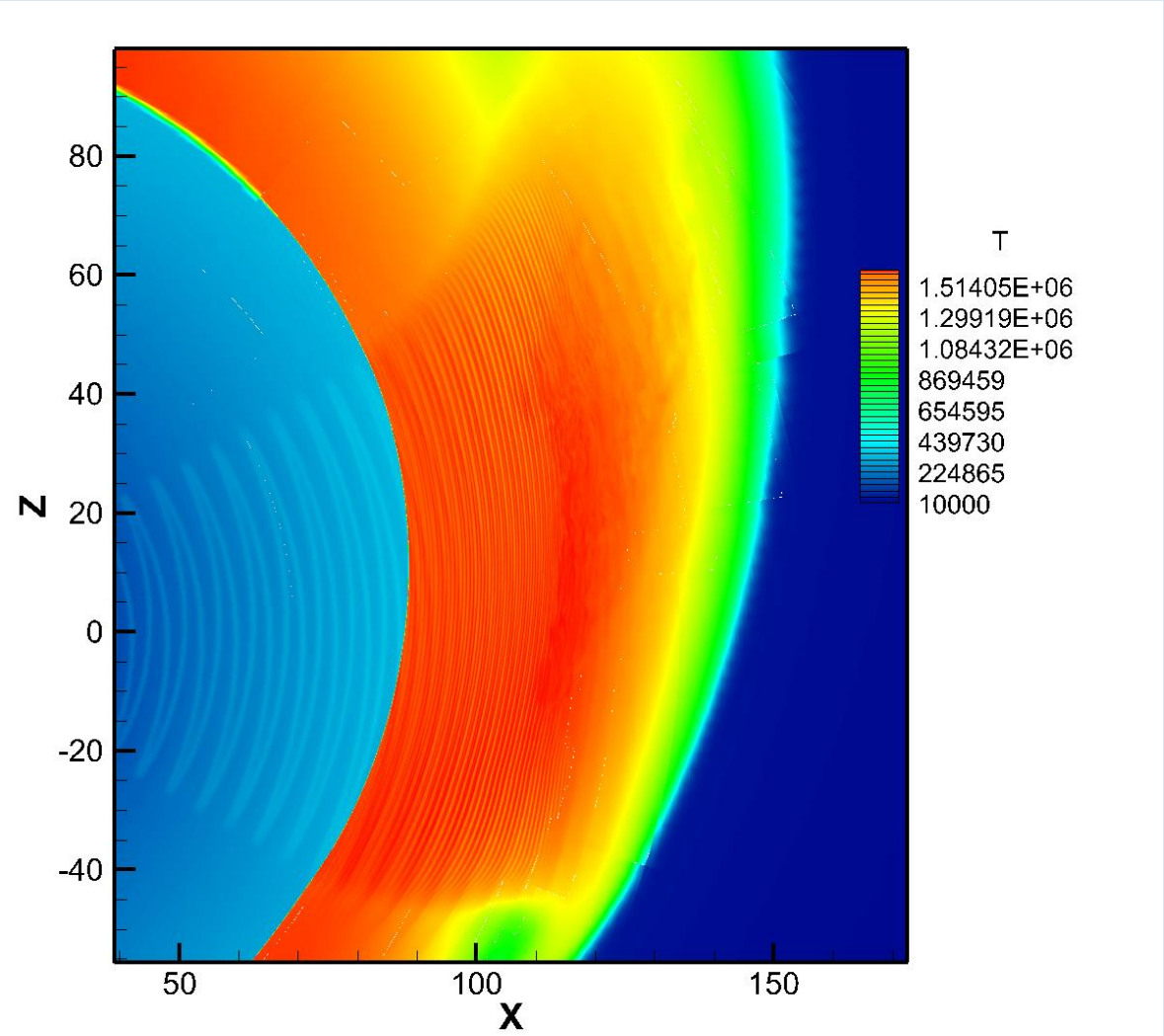

Magnetic field dissipation increases its temperature a little

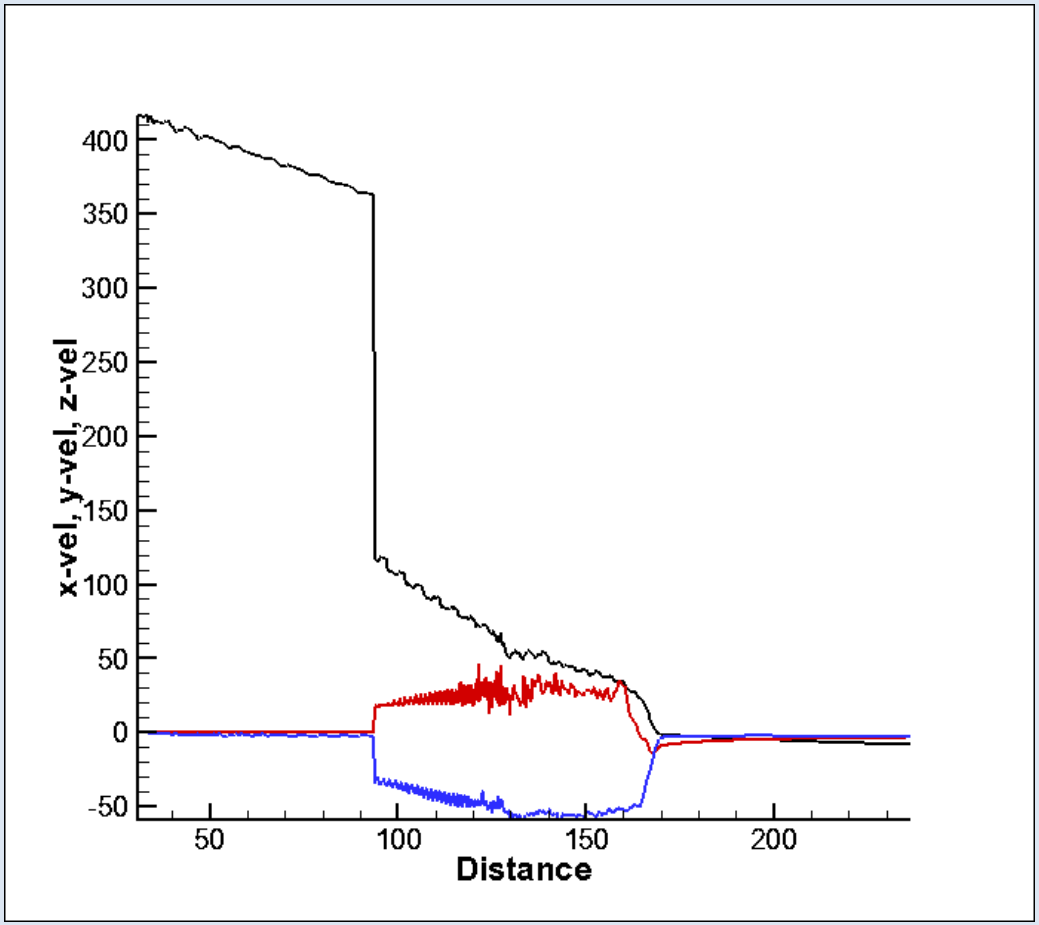

SW velocity components along the V1 trajectory

Estimates, e.g., by Fahr et al. (1986), the heliopause width is very small (< 0.01 AU) if only molecular viscosity and/or regular/anomalous resistivity are taken into account. However, mixing can be stronger because of instabilities. Then, the mixing should be "spotty."

1. Kelvin-Helmholtz instability due to the flow shear.

Instability can be either absolute or convective.

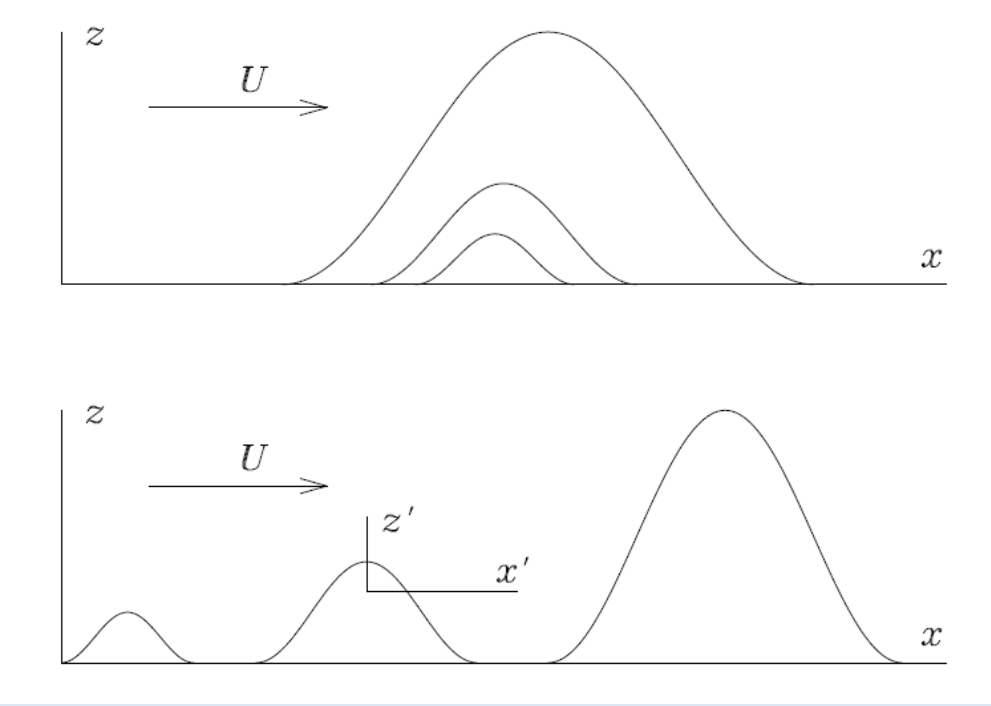

Absolute

Convective

The IVP for a tangential discontinuity is ill-posed (Ruderman & Belov, 2010) : the perturbation increment is unbounded because, for a perturbation harmonic in space, it is proportional to the wavenumber.

For this reason, (i) dissipation should be included or (ii) a smooth velocity profile must be considered. In both cases, the problem becomes well-posed, and it turns that in the velocity threshold for instability decreases (Ruderman & Belov, 2010). Without magnetic field, the HP is unconditionally unstable. In the presence of magnetic field, the HP becomes unstable at some distance from the HP (Ruderman & Fahr, 1995). Chalov (1996) showed stabilizing effect of the HP curvature.

Rayleigh-Taylor instability was suggested by Fahr et al., who blamed on the HP acceleration due to solar cycle.

The role of charge exchange was emphasized by Liewer et al. (1996) and Zank et al. (1999). Axially symmetric studies were performed by Florinski et al. (2005) and Borovikov et al. (2008). However, these are not applicable in 3D, so we performed 3D simulations with space resolution that resulted in the RT unstable HP in axially symmetric formulations.

Heliopause Instability May Strongly Affect Its Shape and the Distribution of Quantities in its Vicinity

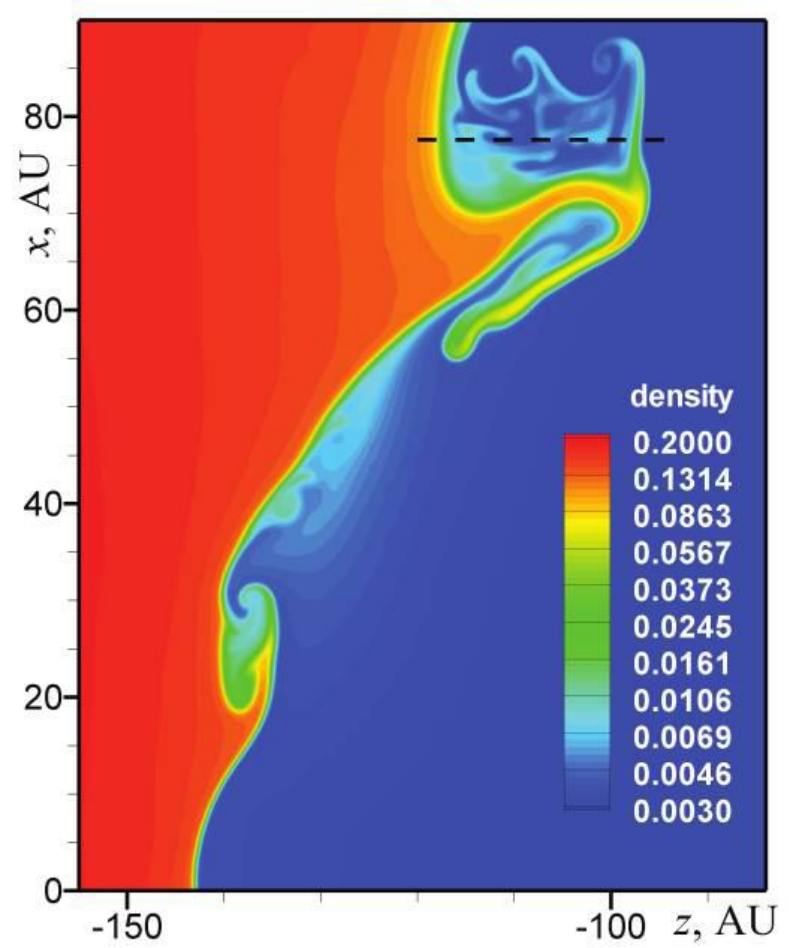

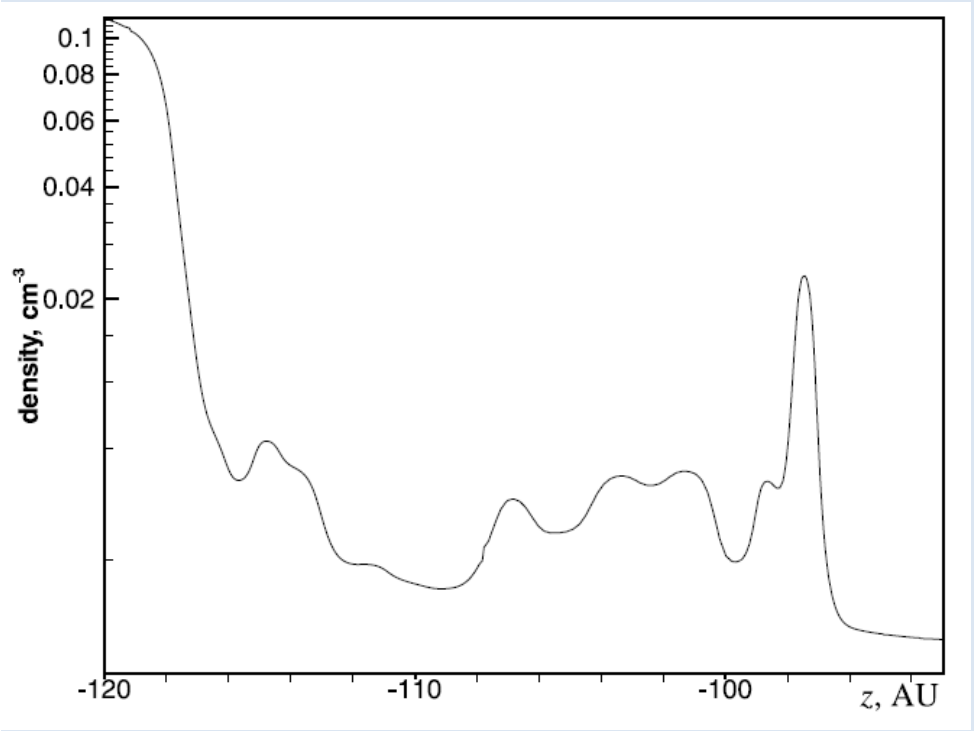

Mixing of the SW and LISM plasma due to the instability (left). The density distribution extracted along the dashed line crossing the mixing region (right) [from Borovikov et al. (2008)].

Solar cycle variations of the SW velocity derived from the Ulysses measurements (Pogorelov et al., 2013)

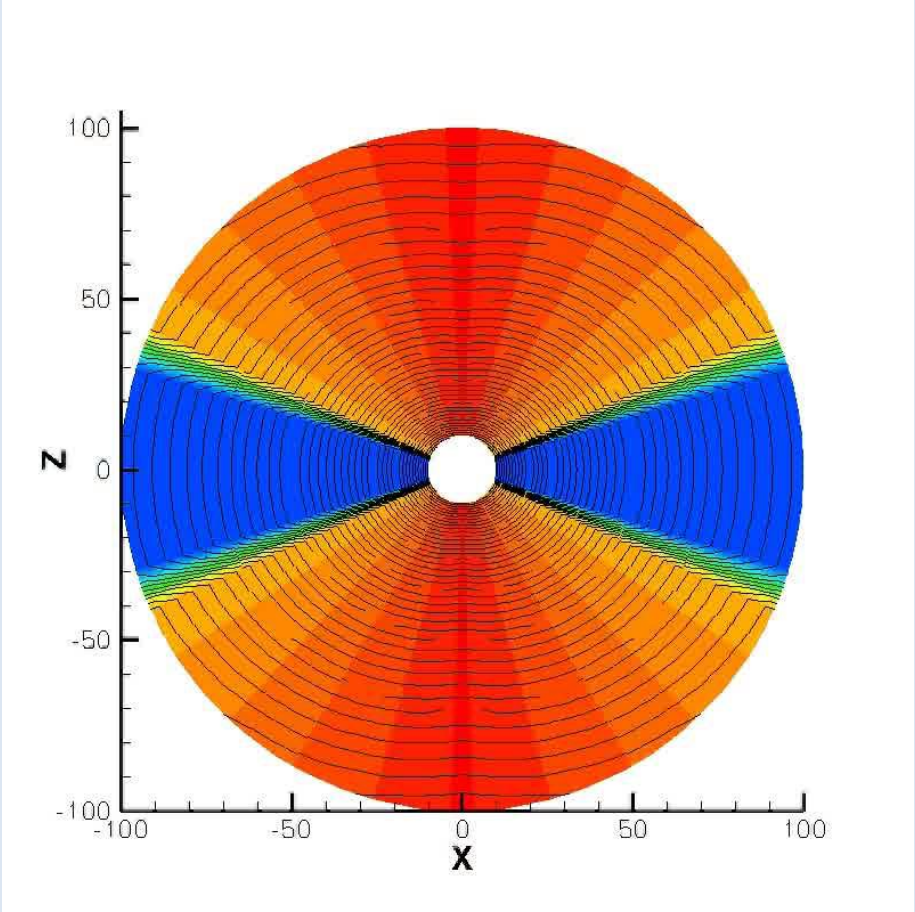

The distribution of the SW radial velocity component in the supersonic region only.

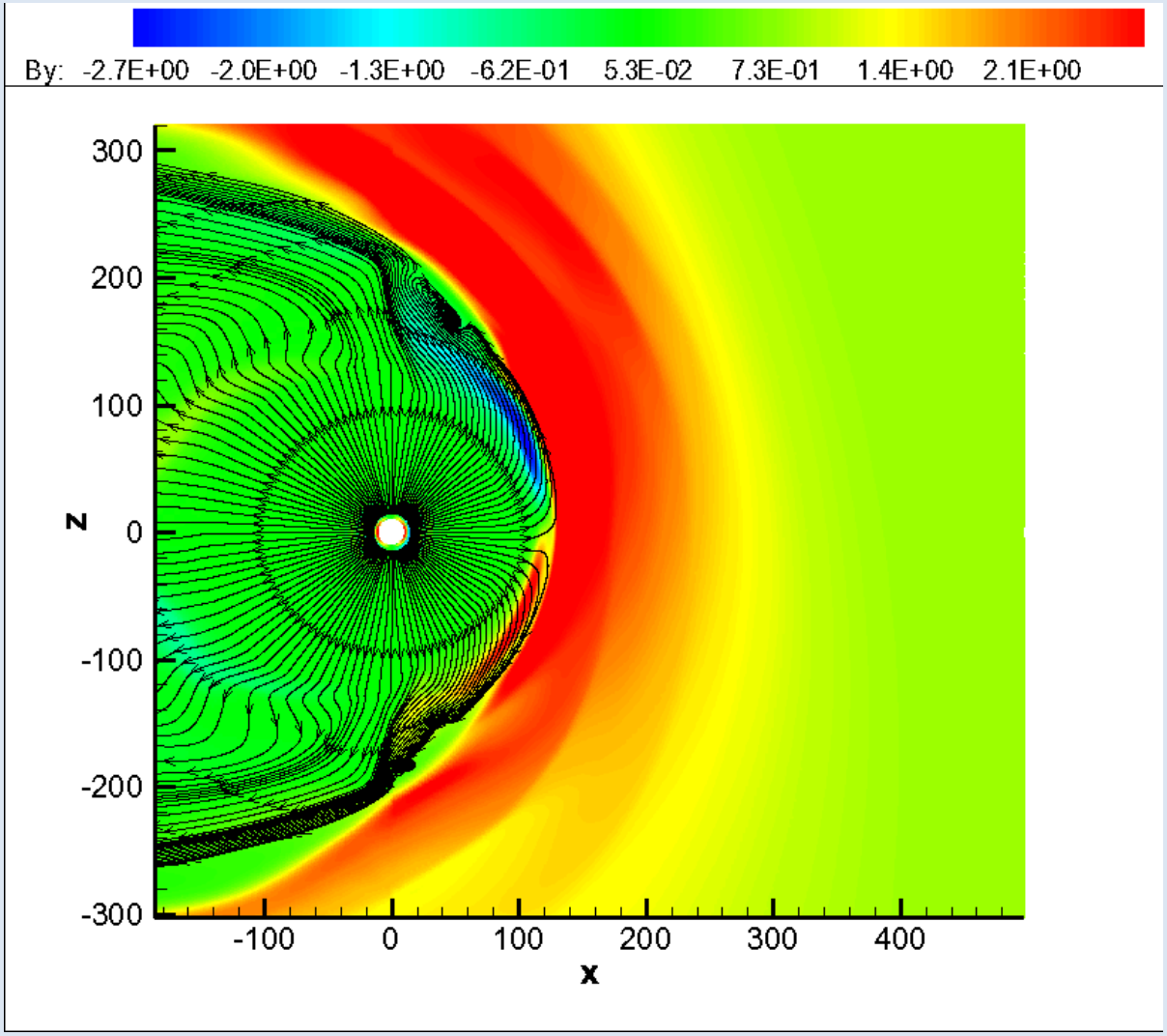

B_y in the meridional plane and SW streamlines

Interaction of the periodic SW with the LISM: Negative radial velocity component and the absence of the latitudinal flow

Parameters for SW-LISM interaction models:

(a) Solar wind at 1AU:

$n_p = 7.4$ cm^{-3} T = 51100 K

$|u| = 450$ km/s B_r = 35μG or 0 μG

(b) The same as (a), but no HMF

(c) The same as (a), but no ISMF

(d) Solar cycle model

Quantity	Slow SW	Fast SW
Number density, n, cm^{-3}	6.9	2.4
Radial velocity component, V, km s^{-1}	450	762
Temperature, T, K	68000	245000
Radial component of the HMF, B_R, nT	3.5	3.5

Local Interstellar Medium at 1AU:

$n_p = 0.08$ cm^{-3} T = 6200 K

$|u| = 23.2$ km/s B_∞ = 3μG $n_H = 0.21$ cm^{-3}

He direction: $\lambda = 79°$, $\beta = 4.9°$

IMF direction: $\lambda = 255°$, $\beta = 44°$

The simulations are performed using a 4-fluid model (one plasma fluid and three neutral atom populations) implemented in Multi-Scale Fluid-Kinetic Simulation Suite (MS-FLUKSS). We use adaptive mesh refinement technique to achieve the resolution of about 0.4 AU in the vicinity of the heliopause

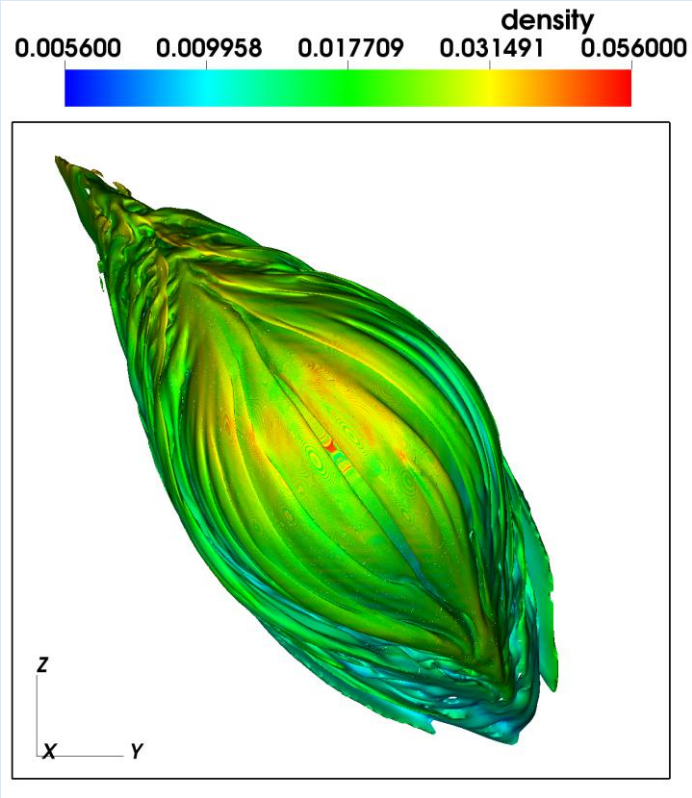

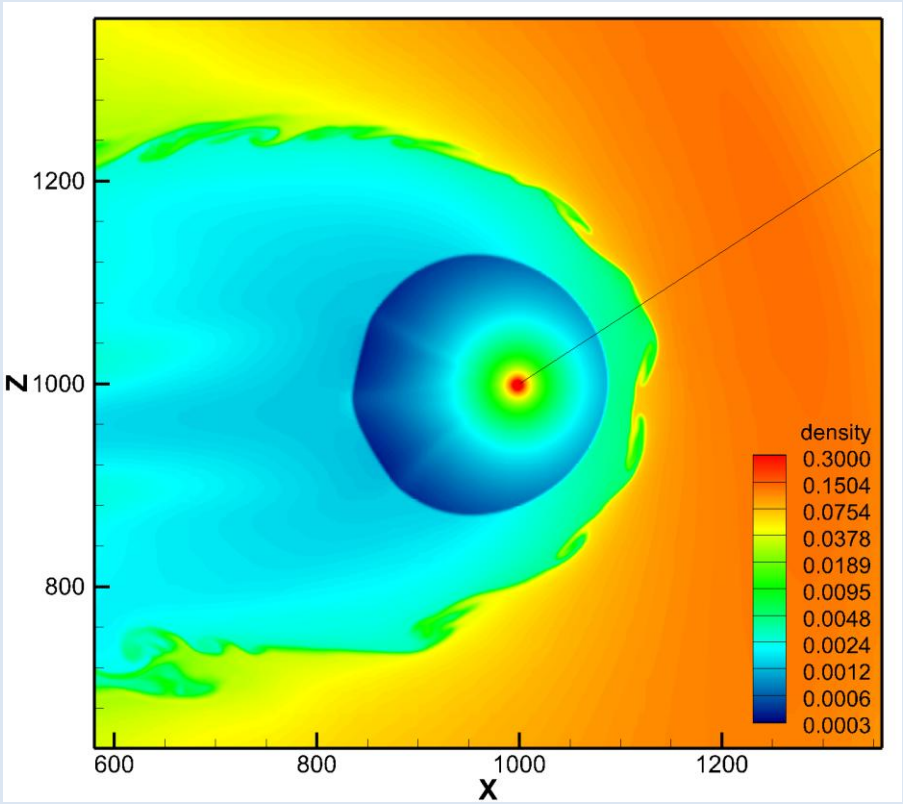

(*Right*) The frontal view of the unstable HP and *(left*) the plasma density distribution in the meridional plane: no HMF (Borovikov & Pogorelov, 2014).

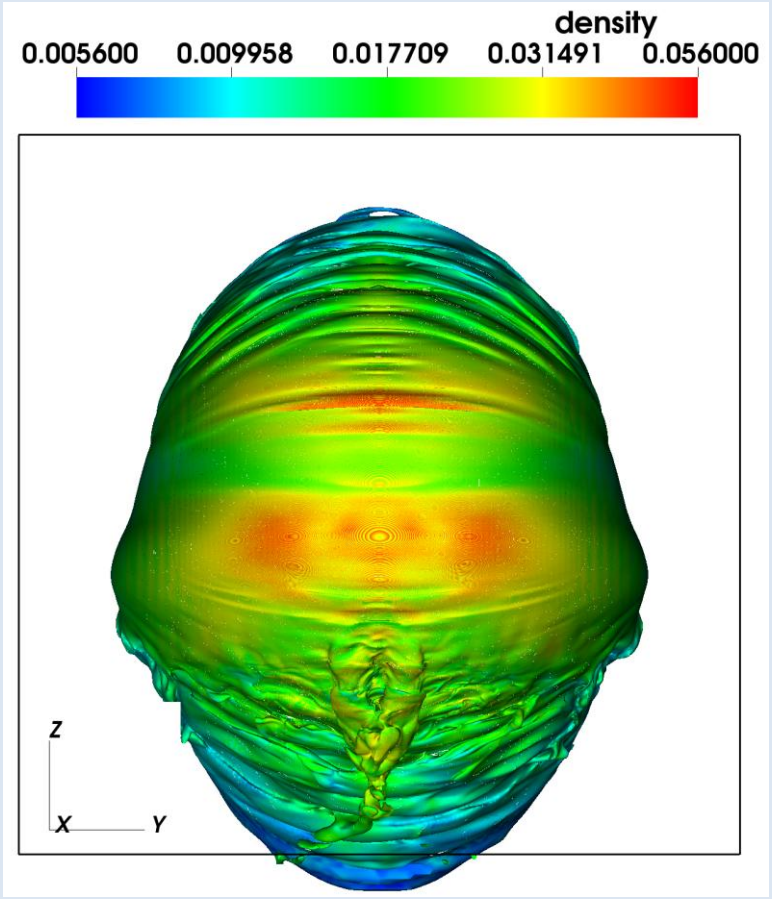

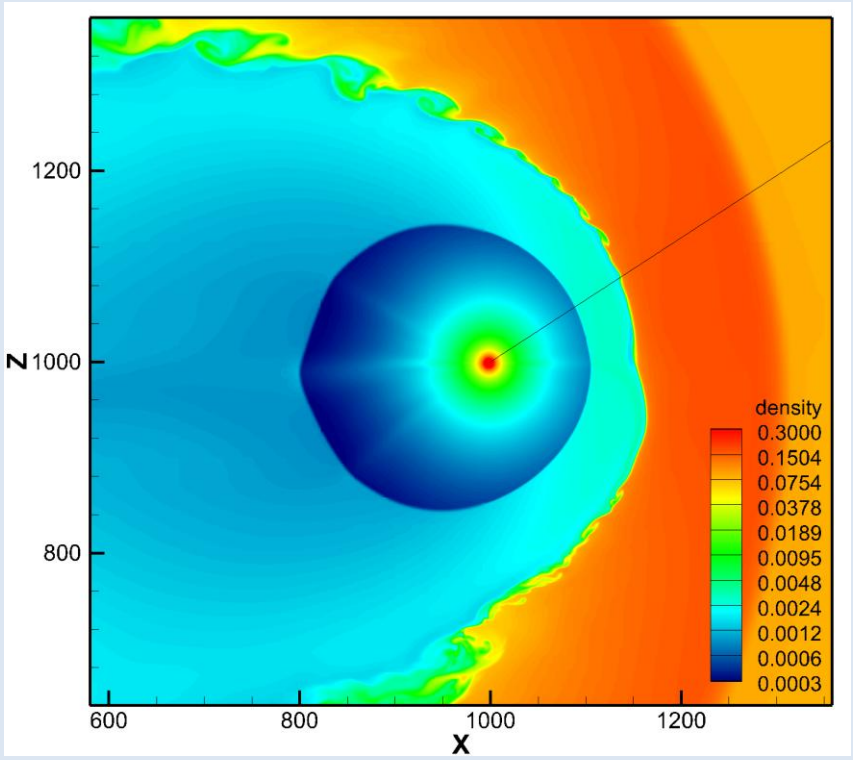

(*Right*) The frontal view of the HP and *(left)* the plasma density distribution in the meridional plane: no ISMF (Borovikov & Pogorelov, 2014).

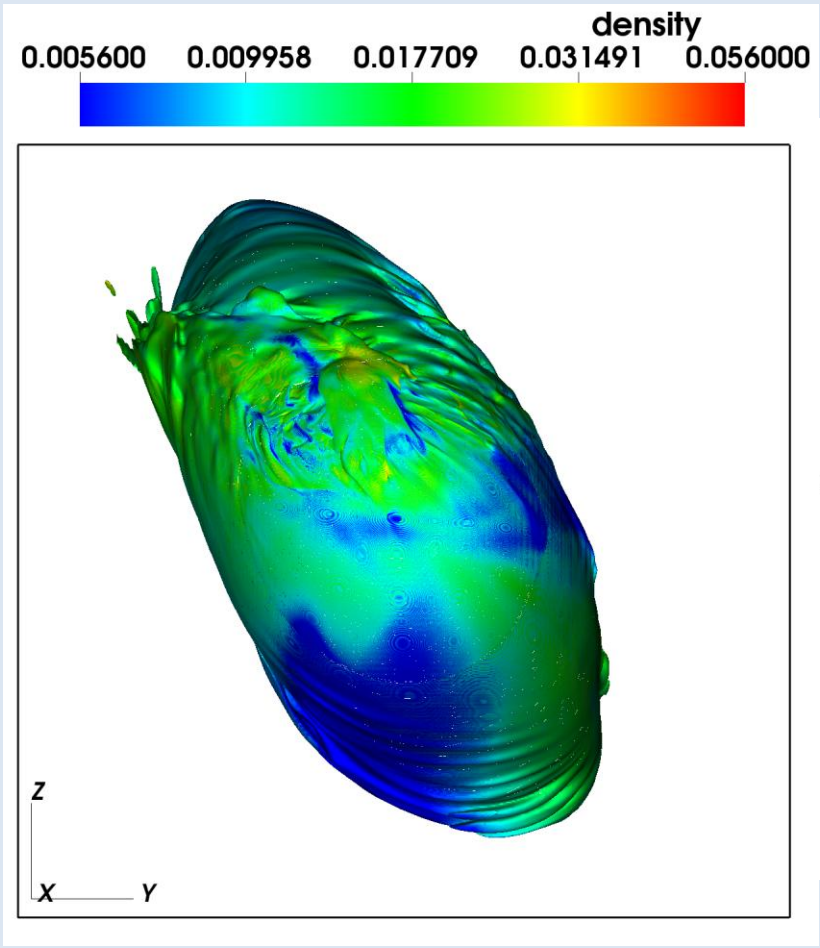

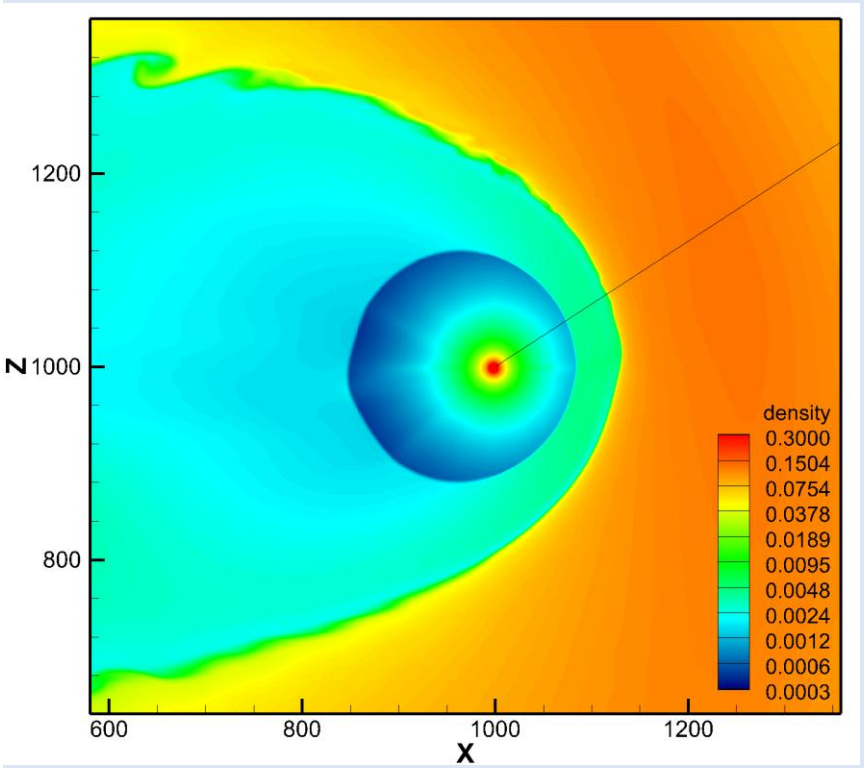

(*Right*) The frontal view of the HP and *(left*) the plasma density distribution in the meridional plane: HMF and ISMF (0.3 nT) (Borovikov & Pogorelov, 2014).

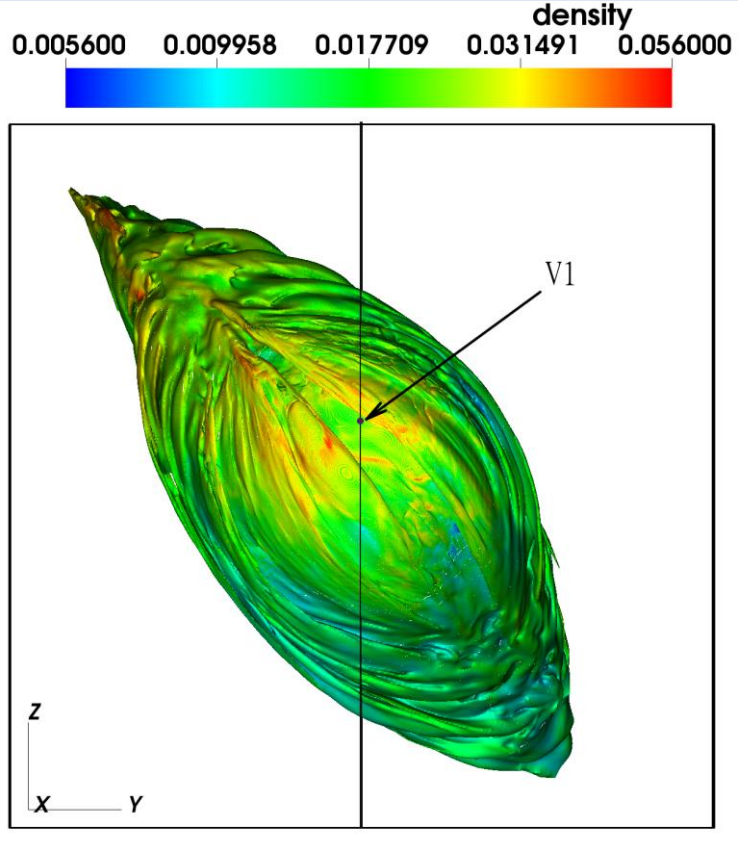

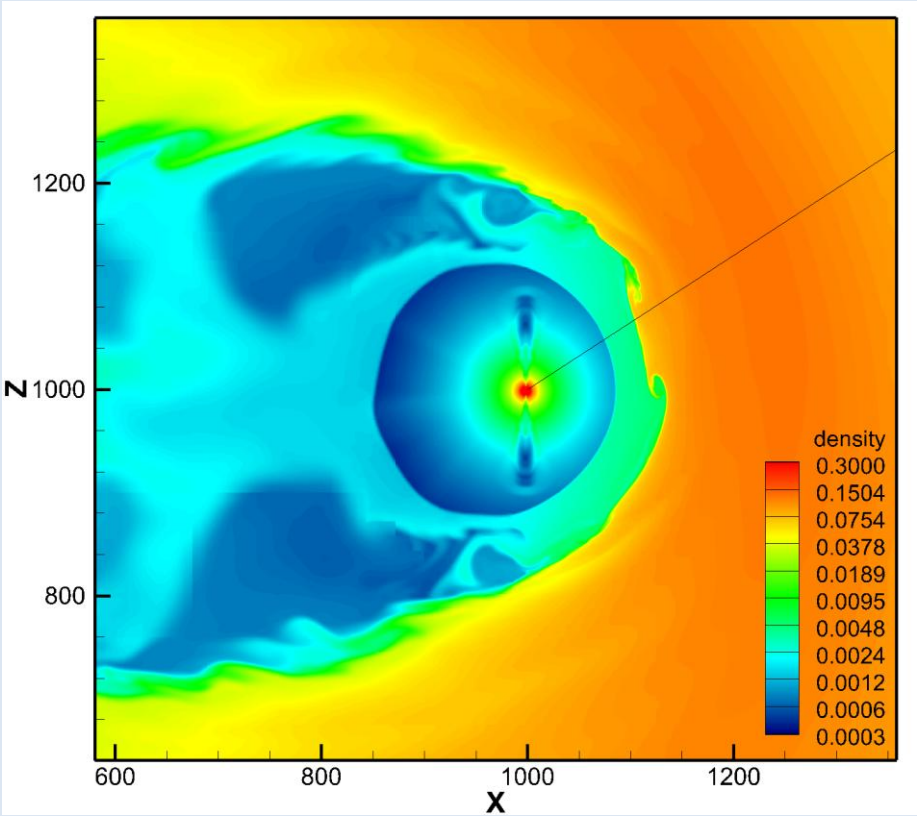

(*Right*) The frontal view of the HP and *(left*) the plasma density distribution in the meridional plane: solar cycle (Borovikov & Pogorelov, 2014).

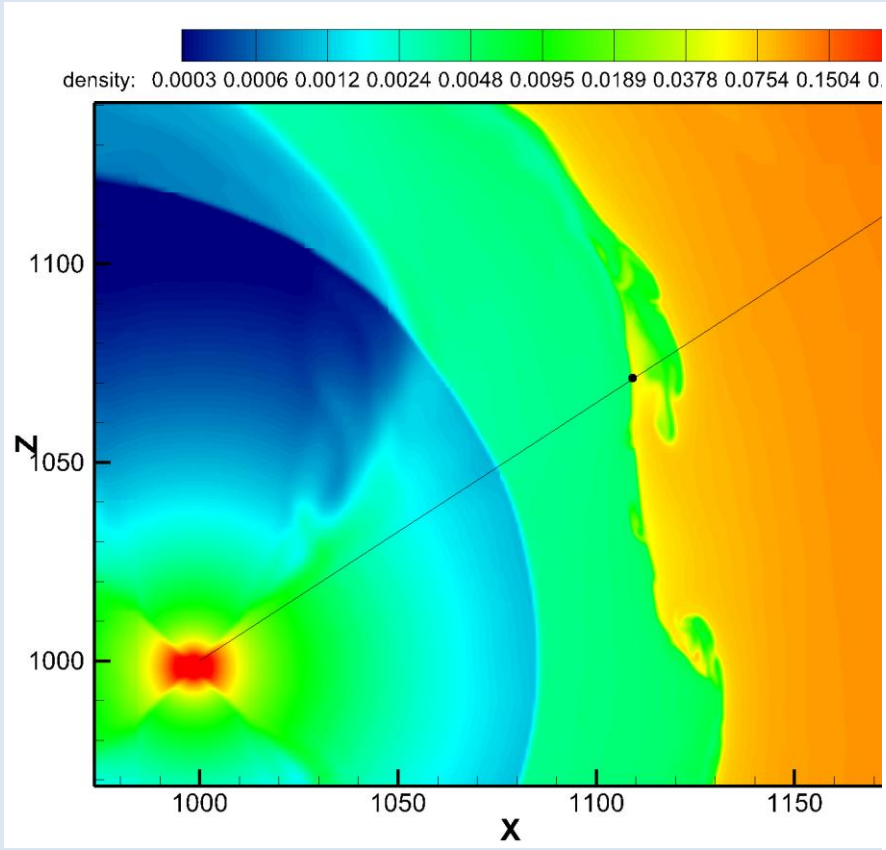

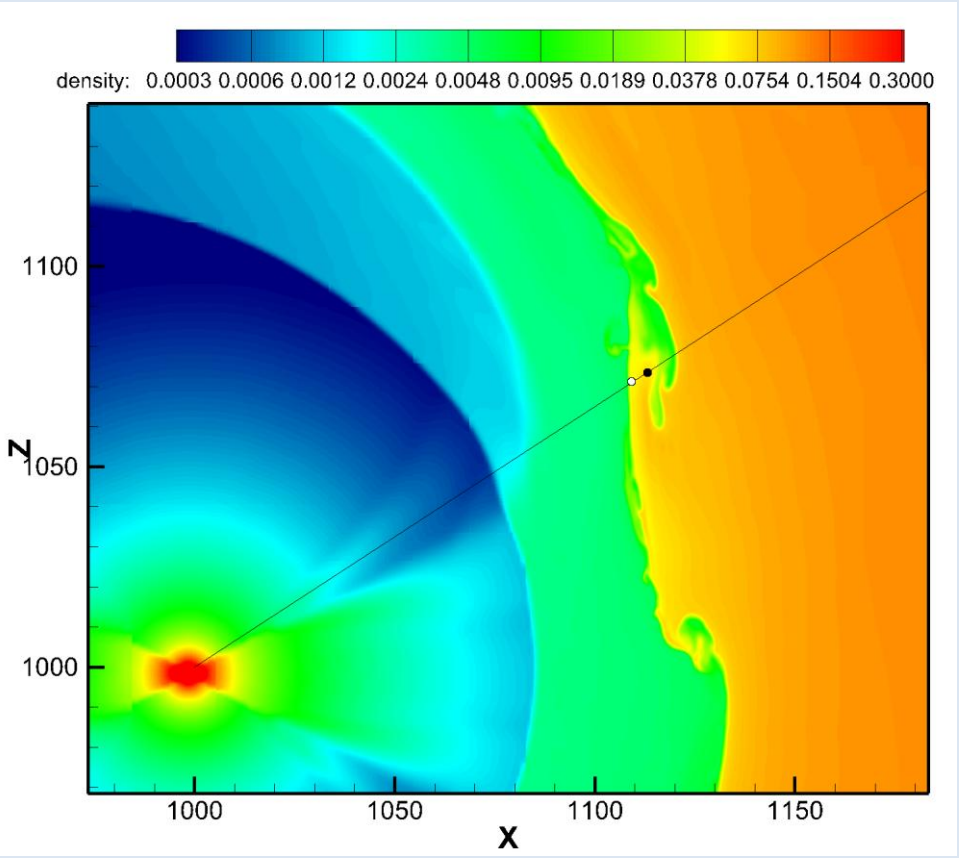

Voyager 1 positions with a two-year interval

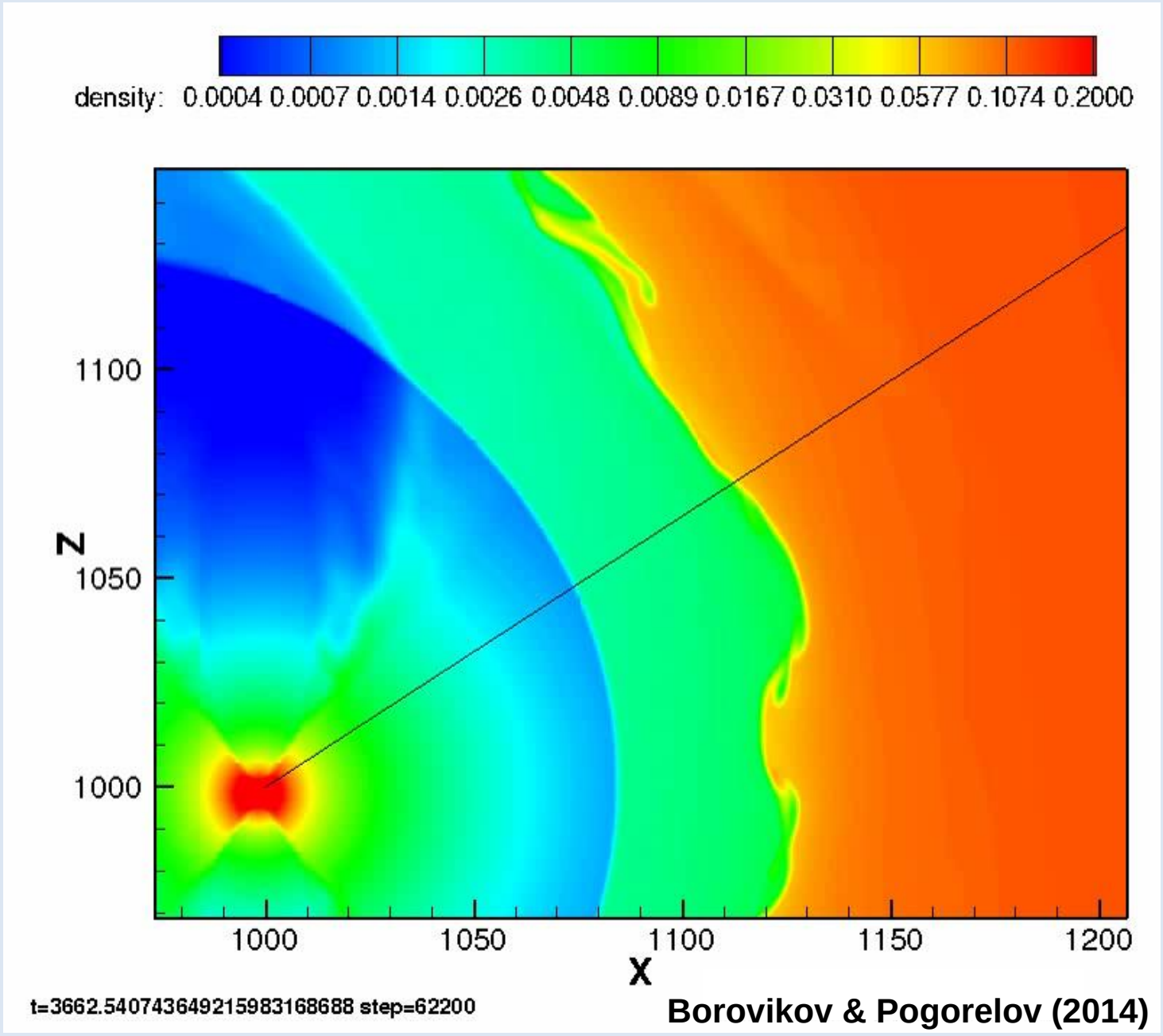

Borovikov & Pogorelov (2014)

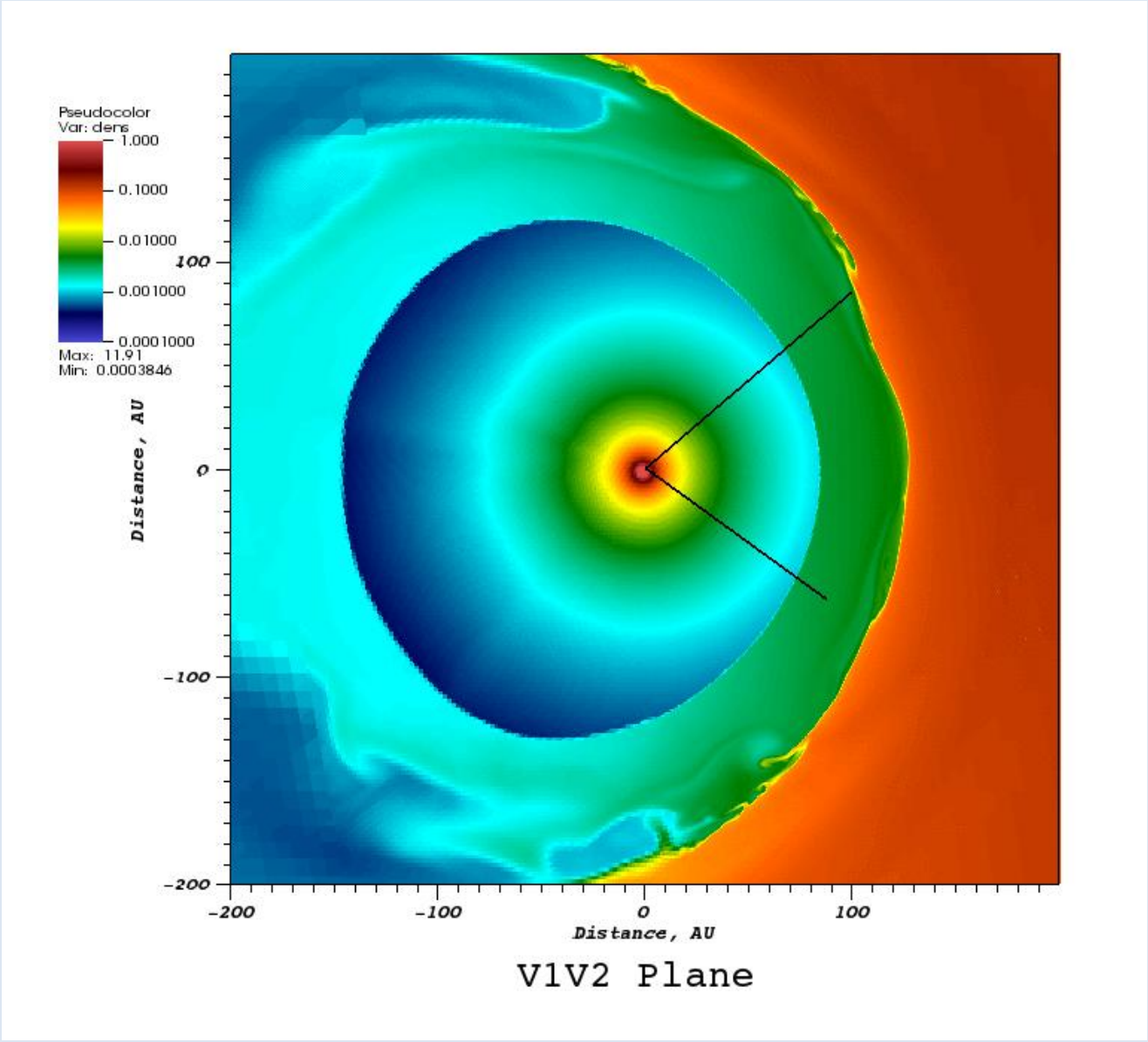
Pseudocolor
Var: dens
1.000
0.1000
0.01000
0.001000
0.0001000
Max: 11.91
Min: 0.0003846
Distance, AU
100
0
-100
-200
-200
-100
0
100
Distance, AU

V1V2 Plane

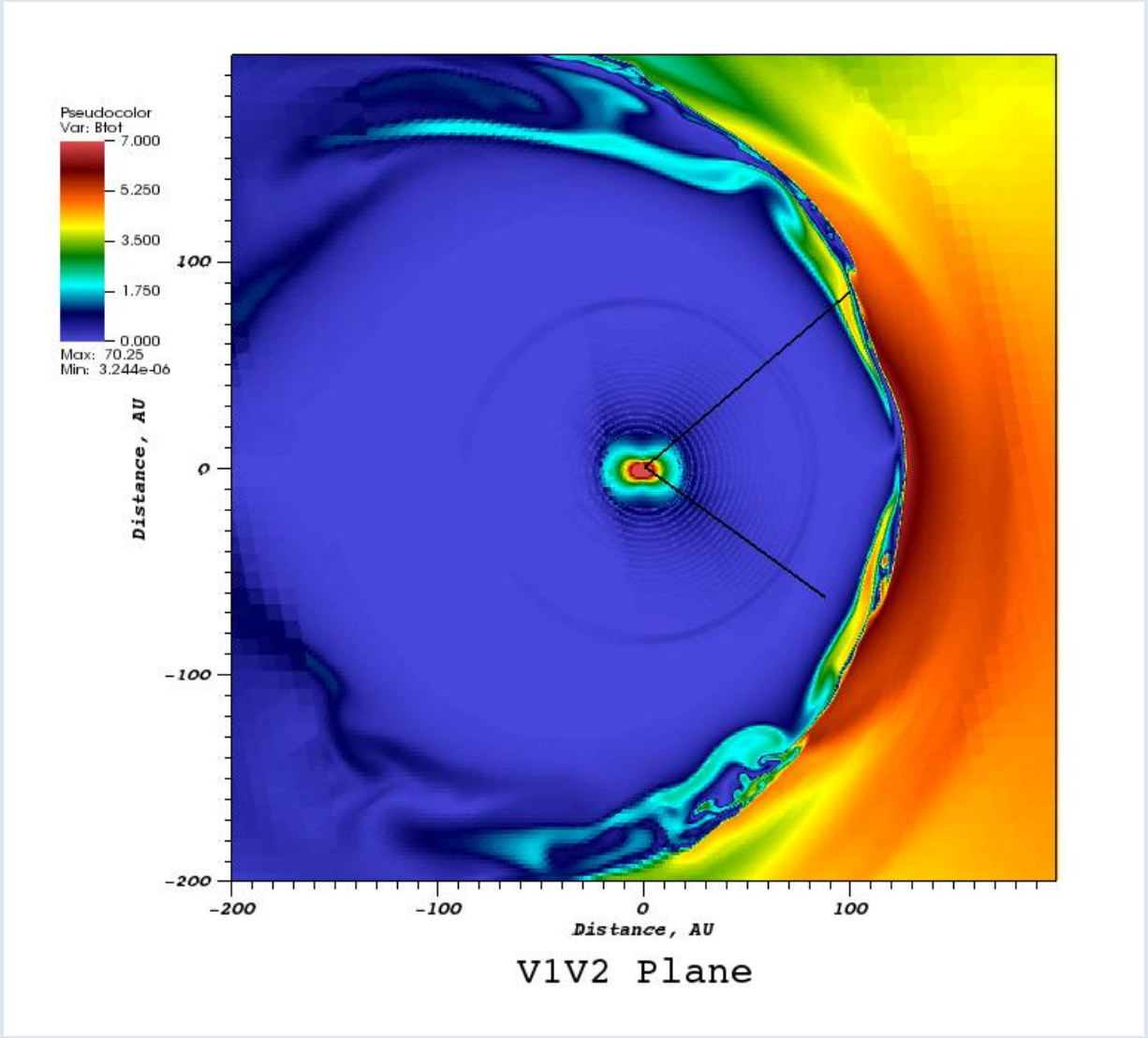
Pseudocolor
Var: Btot
7.000
5.250
3.500
1.750
0.000
Max: 70.25
Min: 3.244e-06
Distance, AU
100
0
-100
-200
-200
-100
0
100
Distance, AU

V1V2 Plane

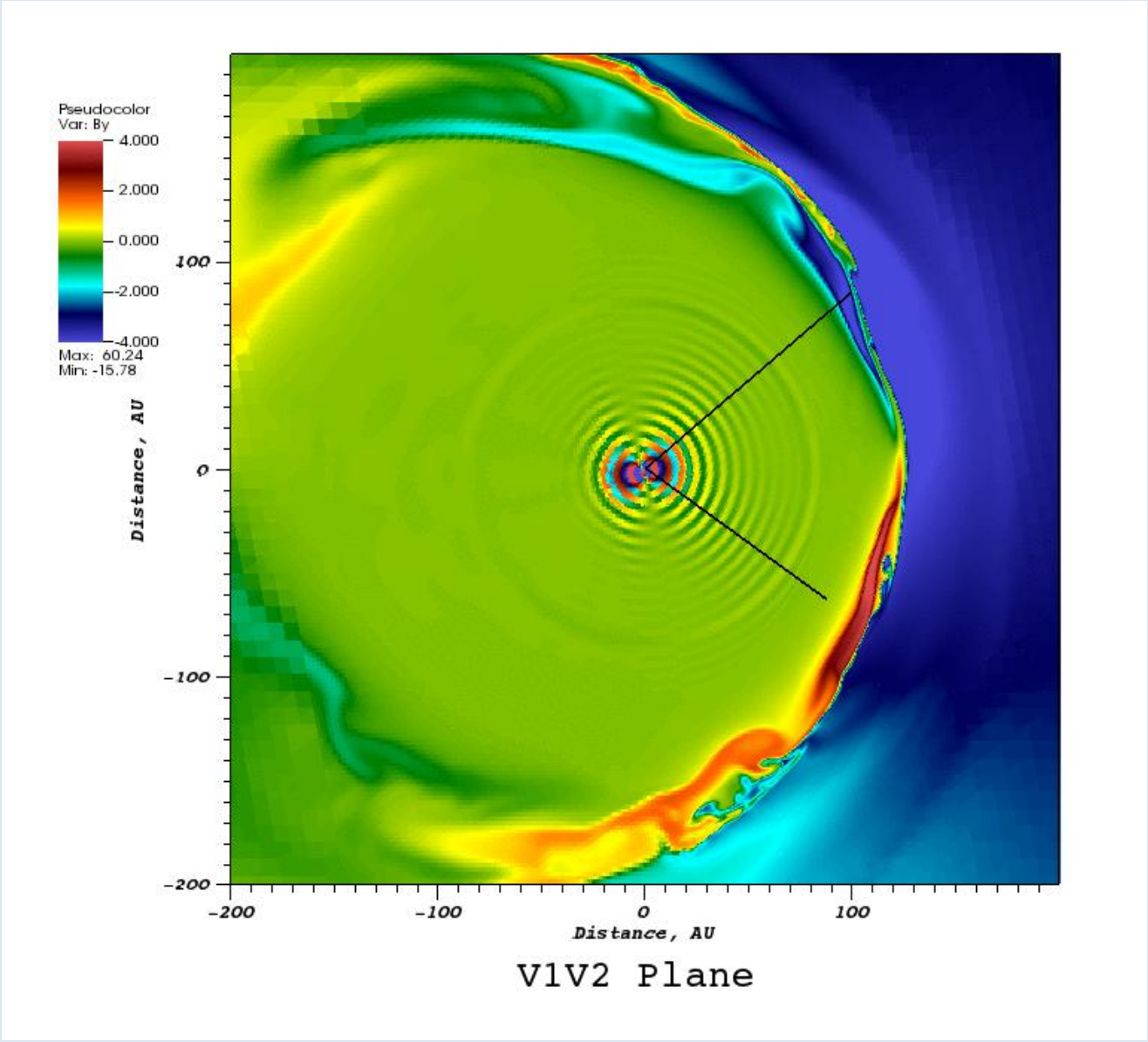
Pseudocolor
Var: By
4.000
2.000
0.000
-2.000
-4.000
Max: 60.24
Min: -15.78
Distance, AU
100
0
-100
-200
-200
-100
0
100
Distance, AU

V1V2 Plane

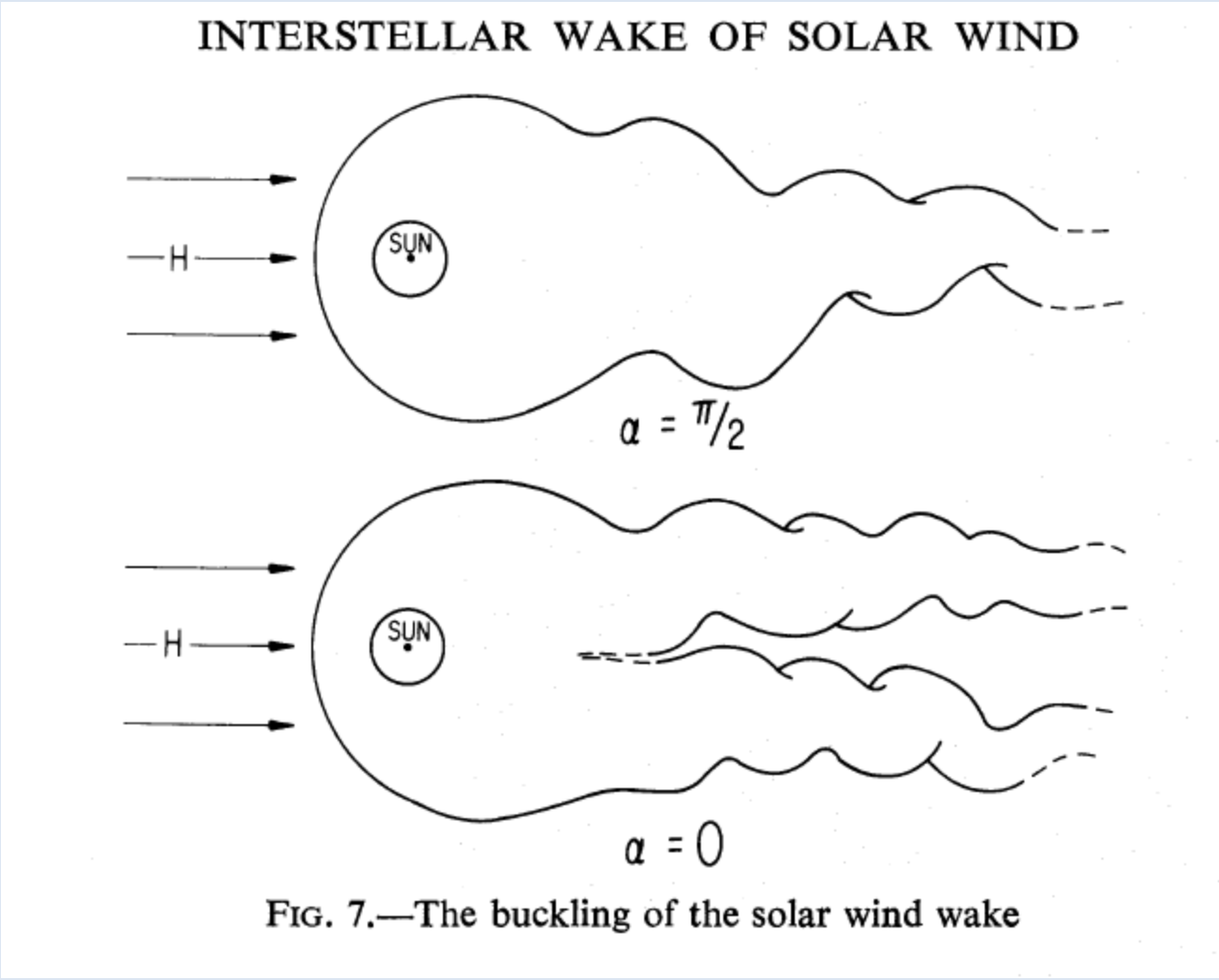

FIG. 7.—The buckling of the solar wind wake

From Yu (1974)

Simulations with the Boundary Conditions from Opher et al. (2015): Unipolar HMF Model, or Why Would the SW have a two-lobe structure?

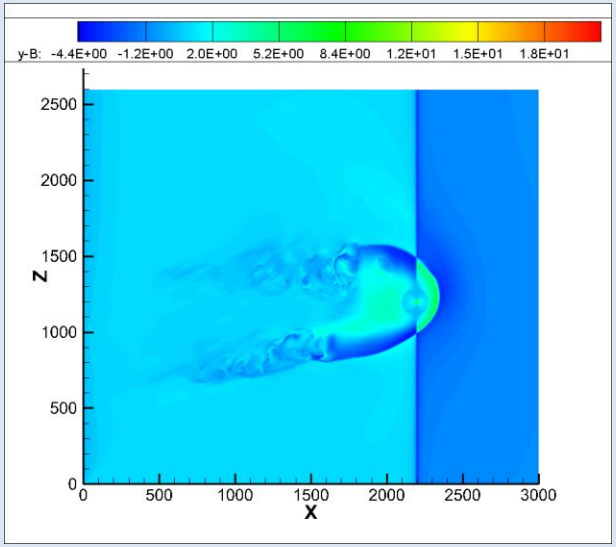

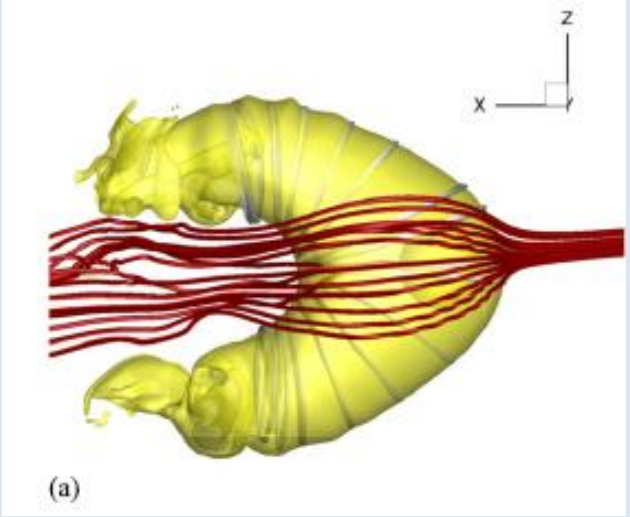

The toroidal component of magnetic field is similar to multi-fluid simulations of Opher et al. (2015). This feature disappears when neutral atoms are treated kinetically.

Our simulations with parameters from Opher et al. (2015) with B_ISM=0

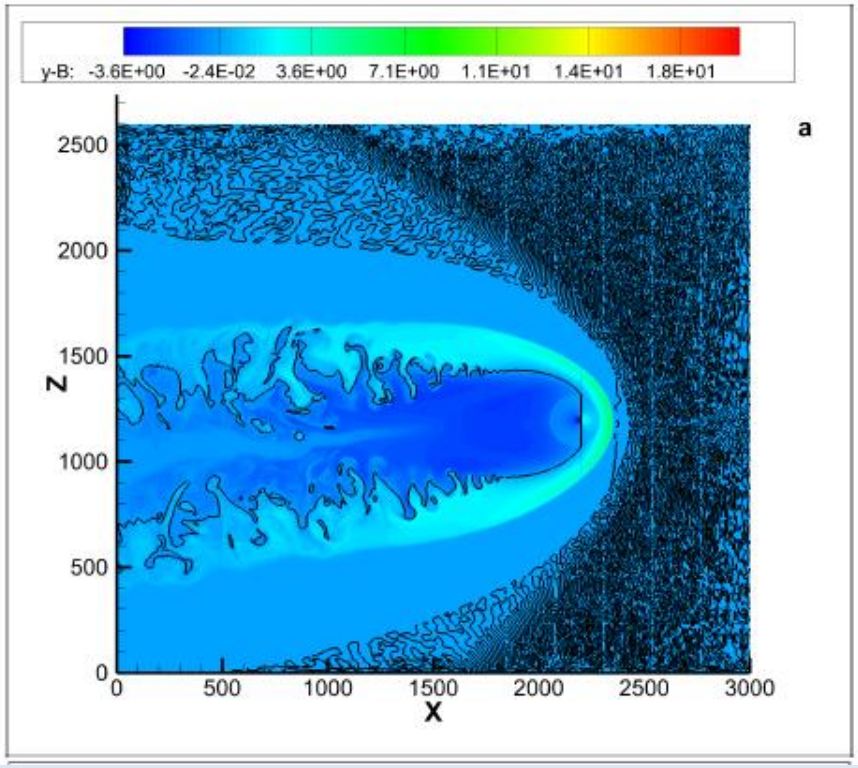

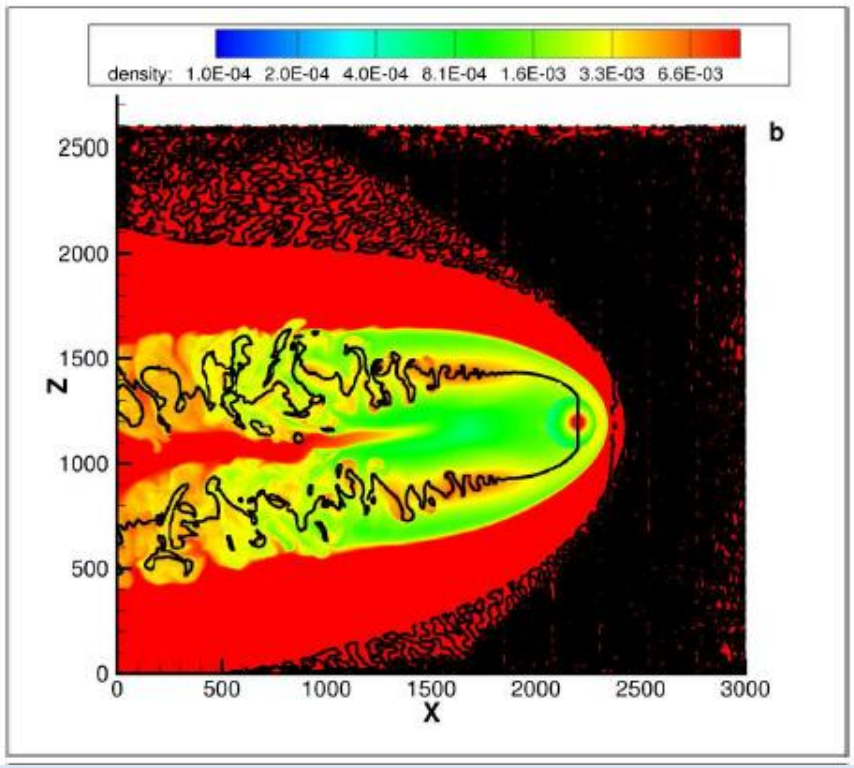

B_y (left) and plasma density (right) in the meridional plane. The black line inside the HP is defined by B_y=0 – the effective center of deflected (initially Parker) spiral field.

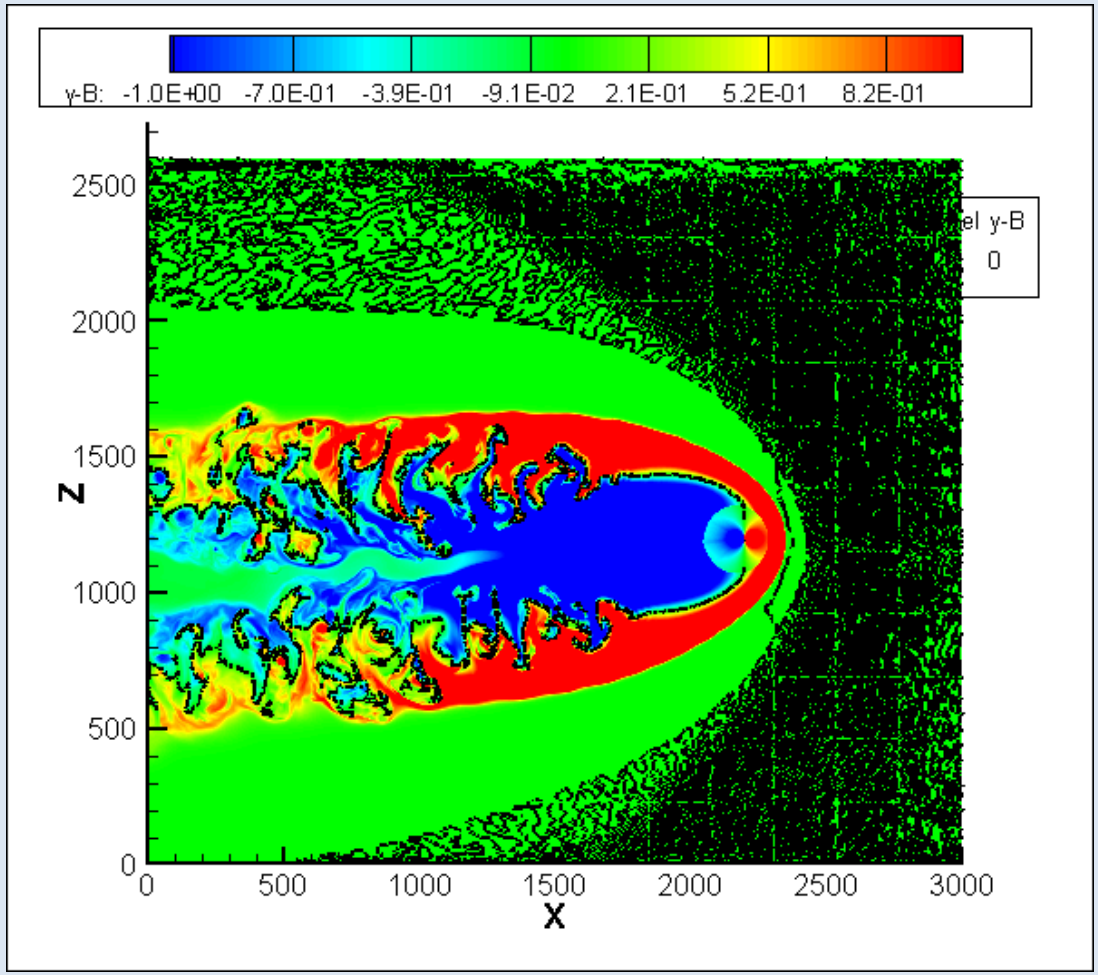

By on a grid twice finer in all directions

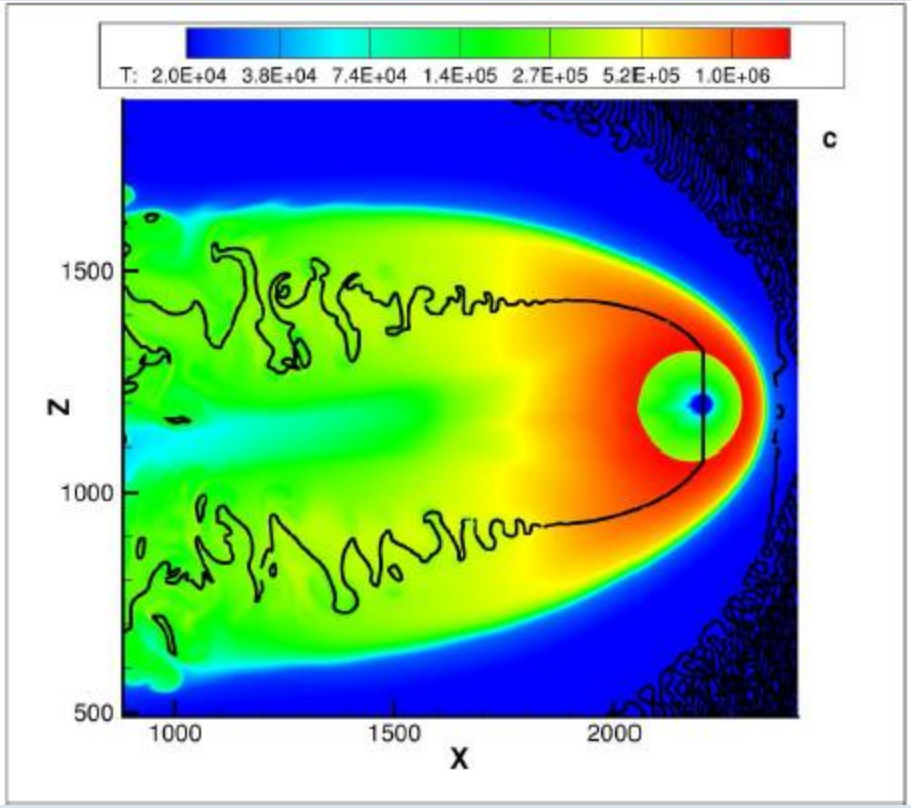

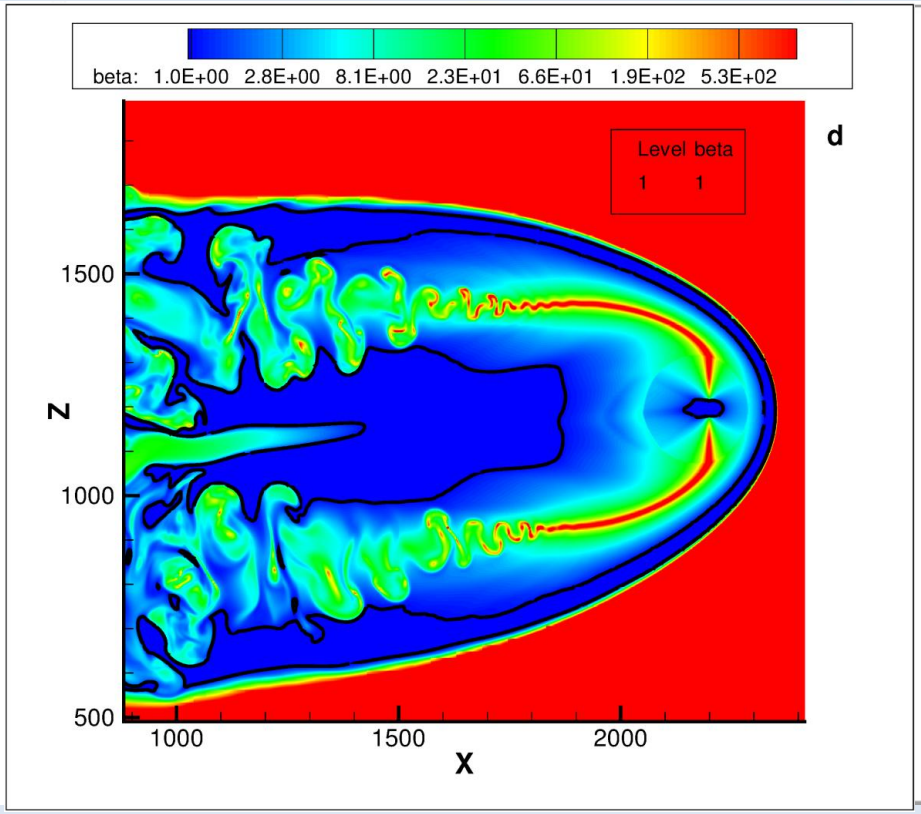

Plasma temperature (left) and plasma beta (right) in the meridional plane. The black line inside the HP in the left panel is defined by B_y=0 – the effective center of deflected (initially Parker) spiral field. The black line in the right panel is defined by β =1.

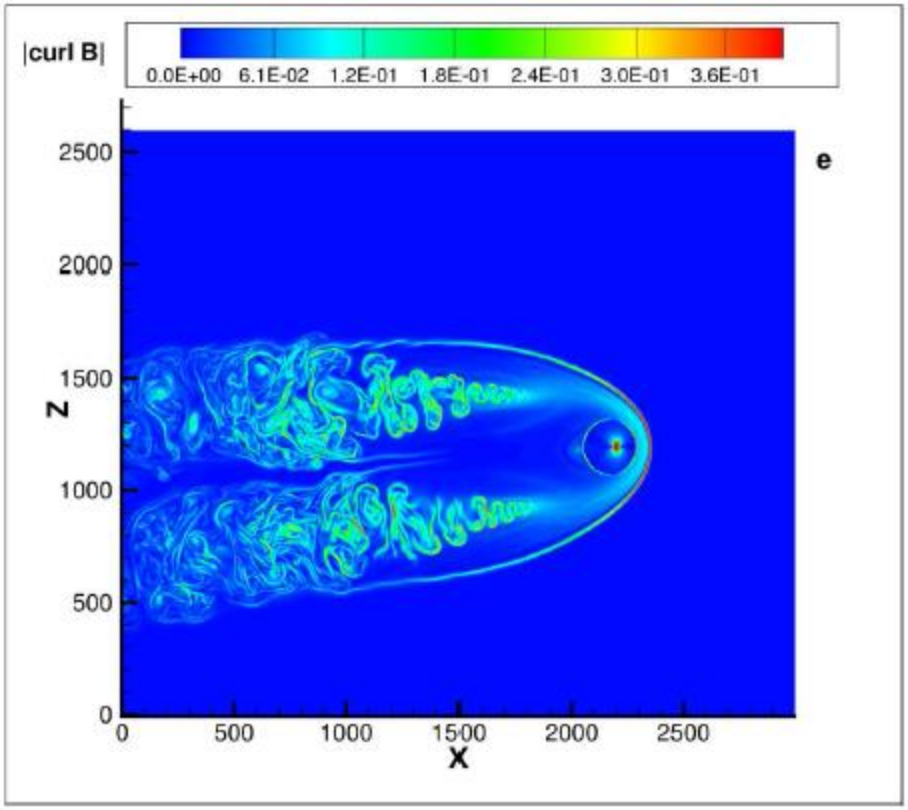

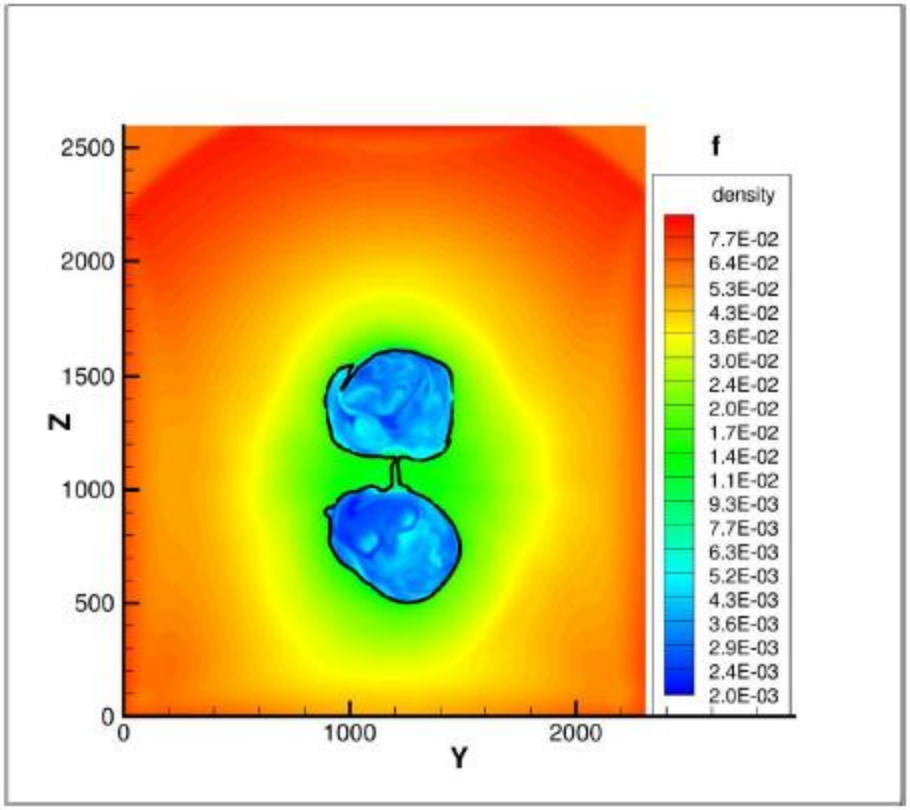

Curl of B (left) in the meridional plane and plasma density at x=200 (right). The black line outlines the HP.

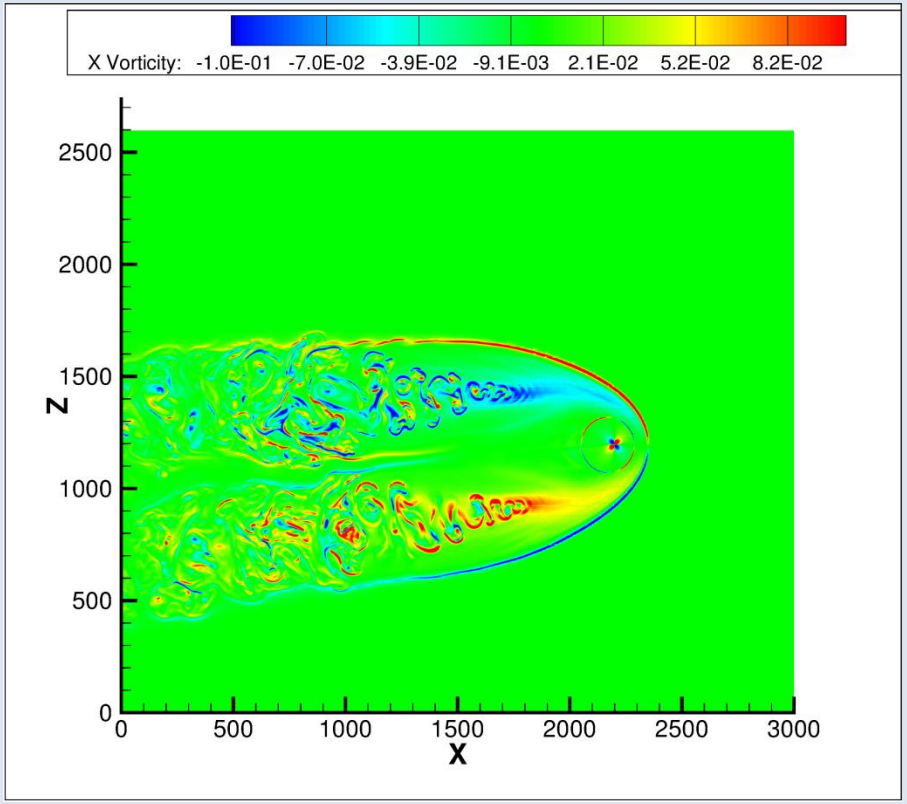

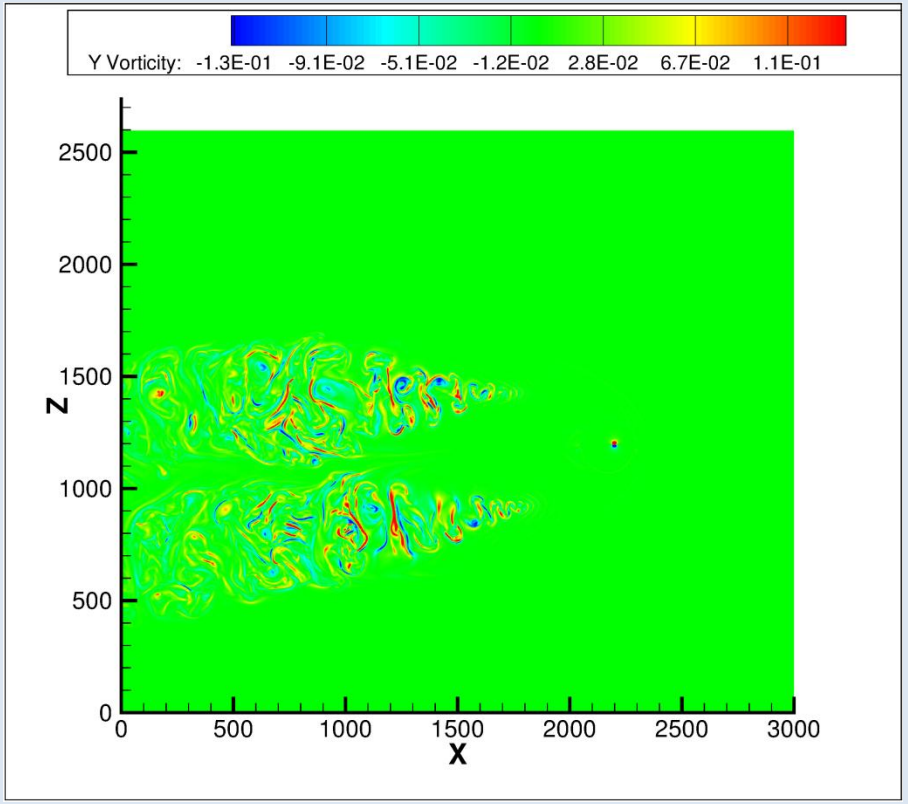

The x- and y-components of the curl B in the meridional plane

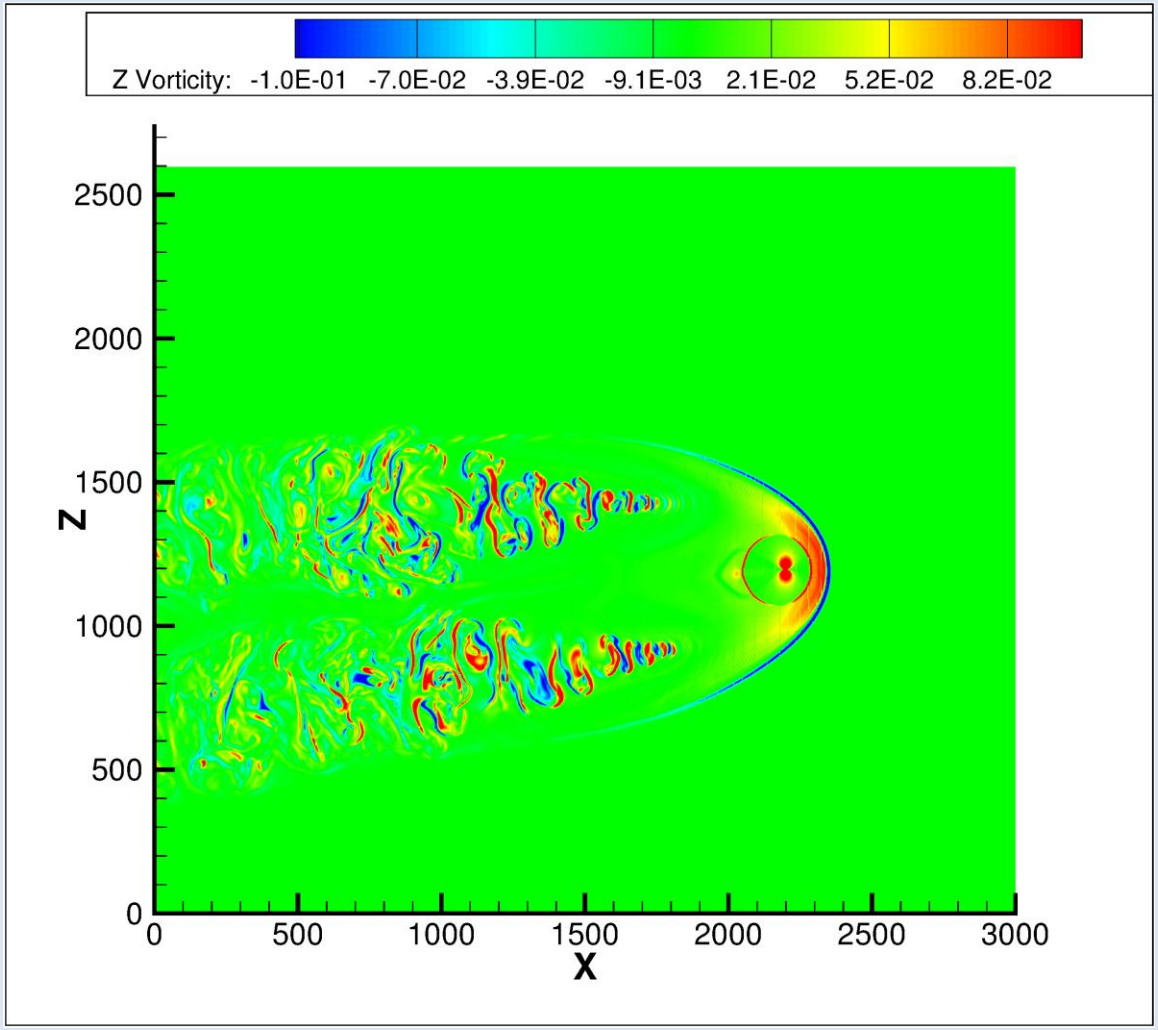

The z-component of the curl B in the meridional plane

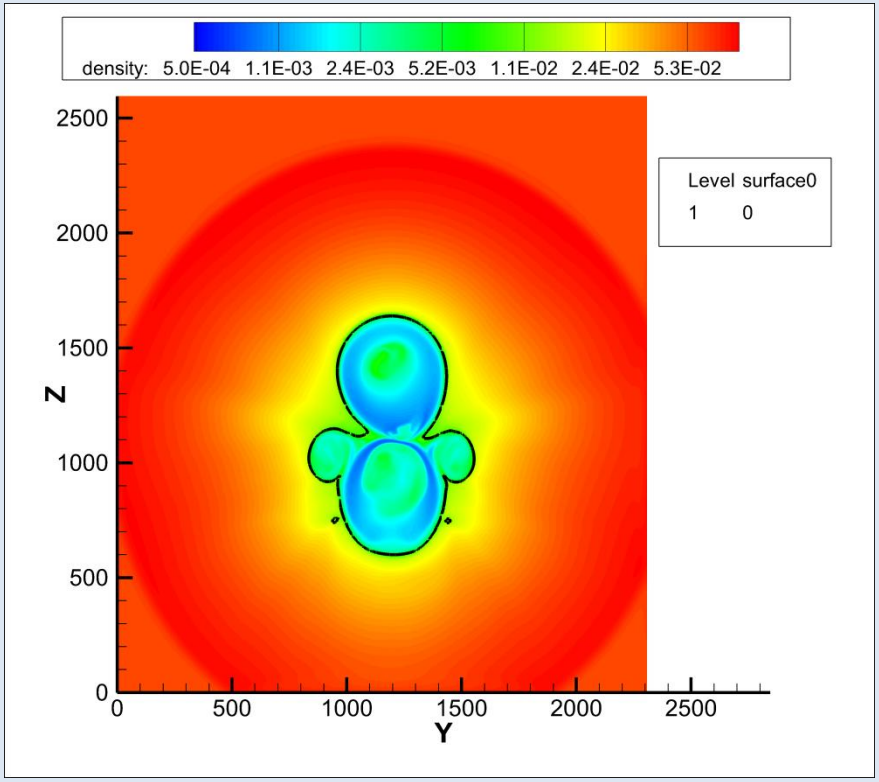

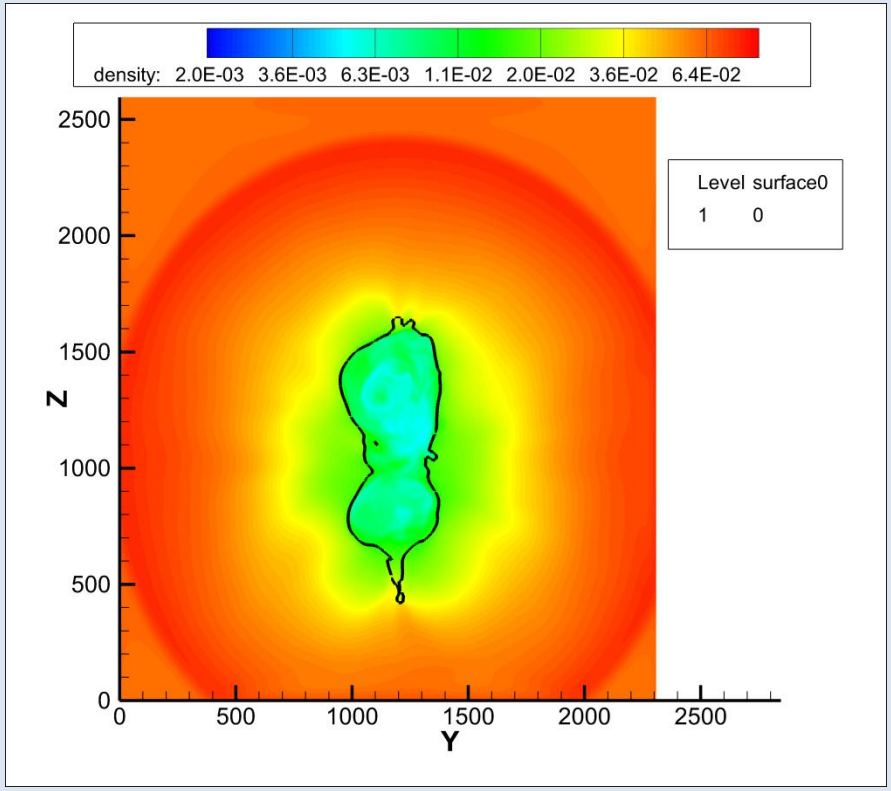

The same problem as in the previous couple of slides, but with genuine Parker field, that is, dipolar with coinciding magnetic and rotation axes (flat current sheet): a simply connected HP without splitting.

5000 AU heliotail with the unipolar IMF and kinetic treatment of H atoms (Pogorelov et al., 2015)

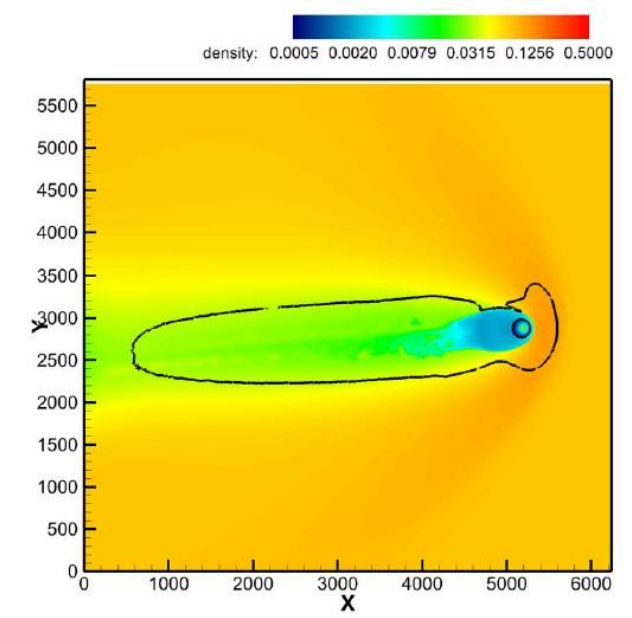

Plasma density in the solar equatorial plane. The black line if defined be the condition M_f=1.

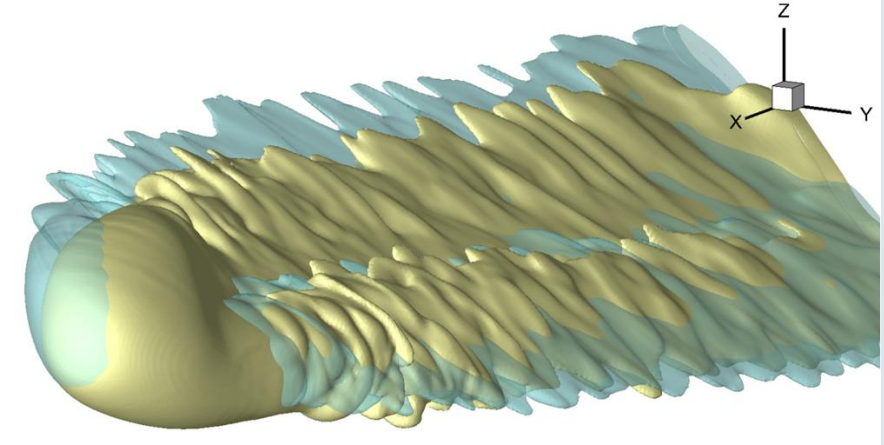

Pogorelov et al. (2013): the HP for B_∞ = 3 μG (yellow) and B_∞ = 4 μG (blue): no two-lobe structure in agreement with Izmodenov et al. (2015).

HMF and ISMF lines: the regular Parker field is destroyed in the tail

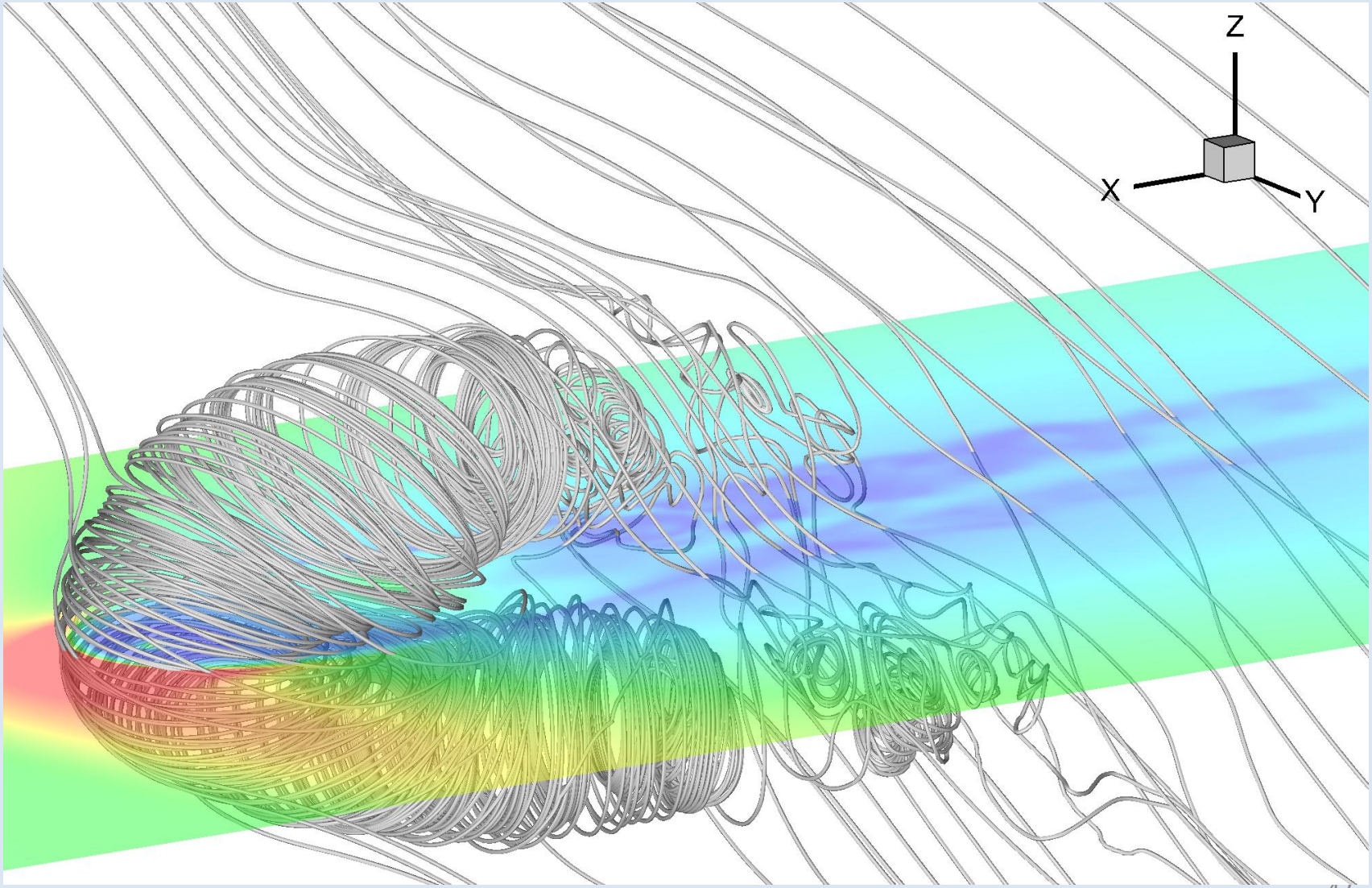

The shift of the heliotail may give more information on the ISMF direction through fitting TeV GCR small-scale anisotropy (Zhang et al. 2014)

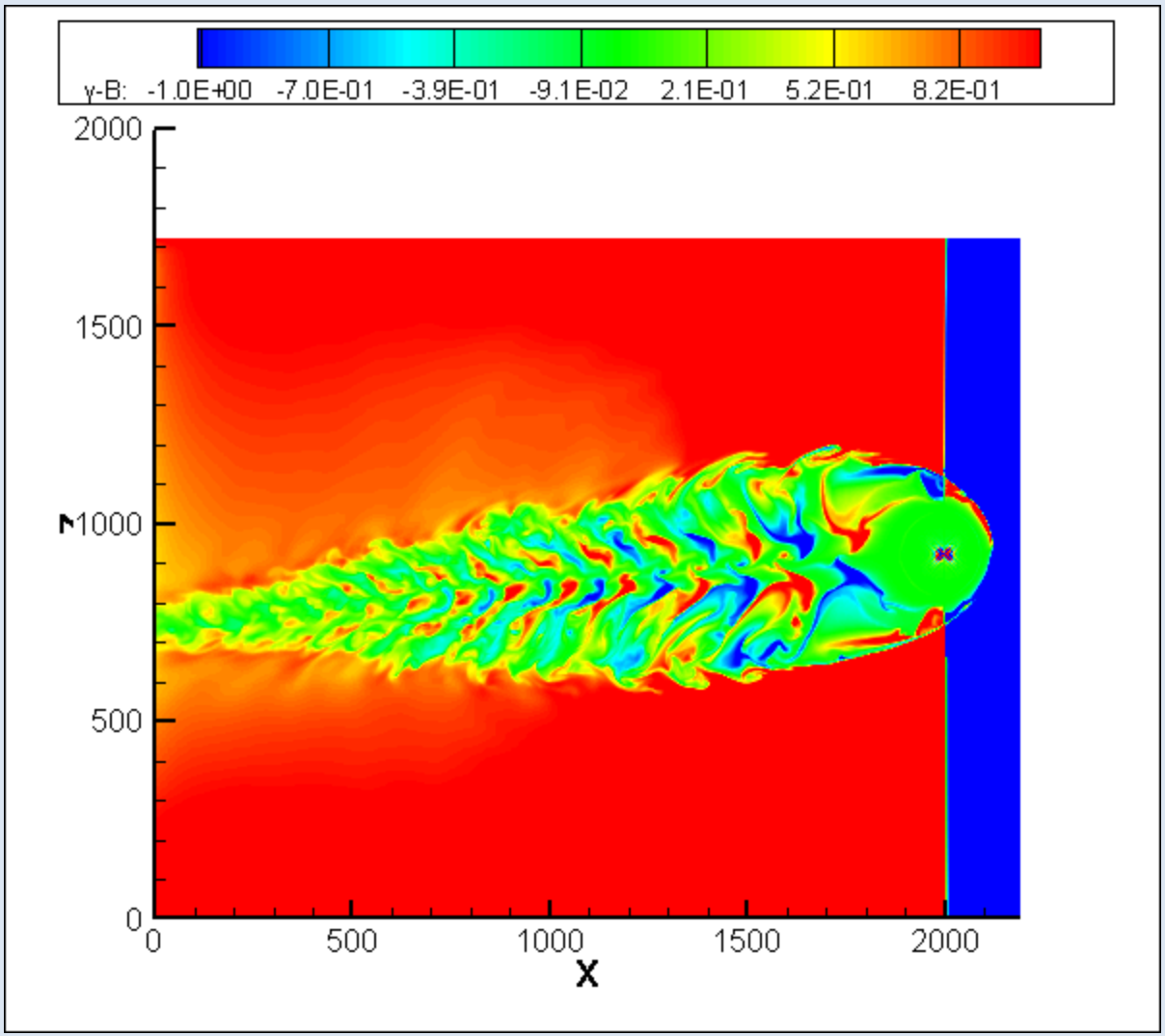

The y- (out-of-plane) component of the magnetic field shows features of solar cycle.

The heliotail with the LISM properties from McComas et al. (2015)

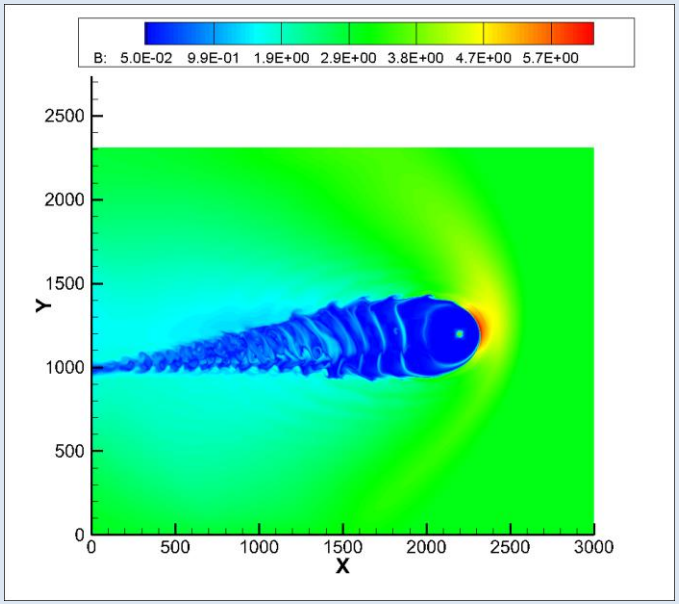

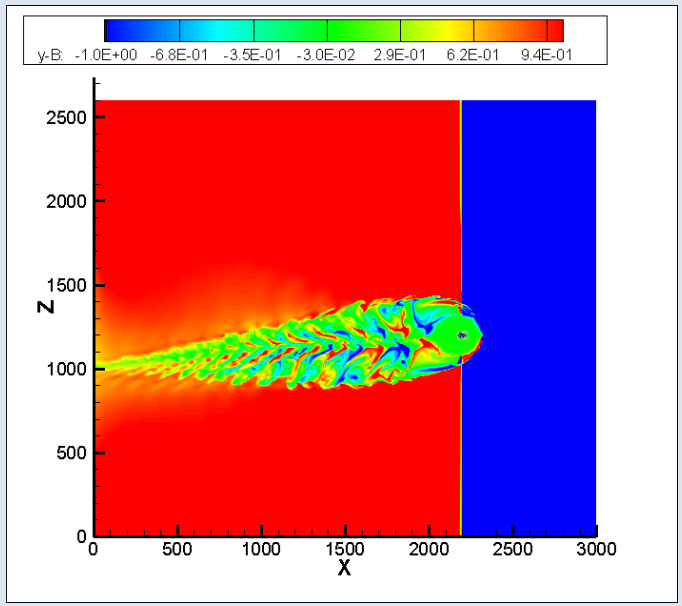

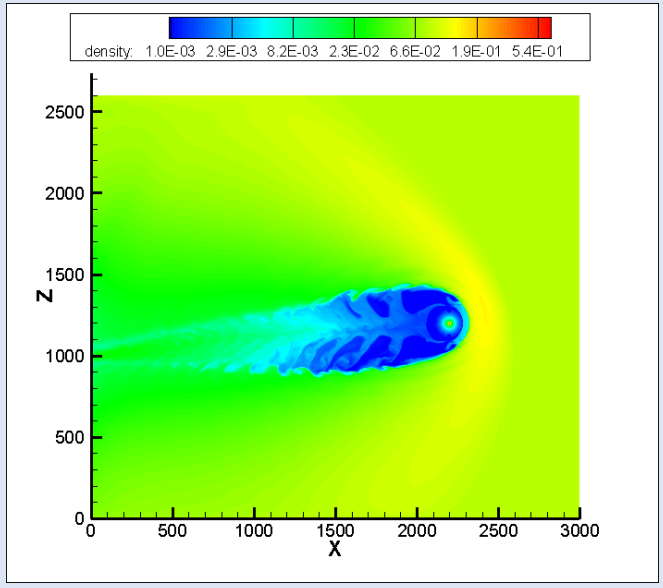

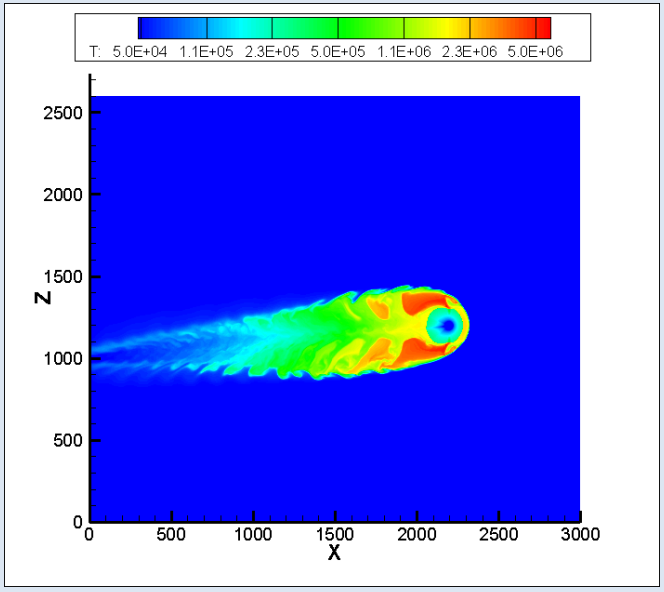

The heliopause from different view angles shows no two-lobe structure

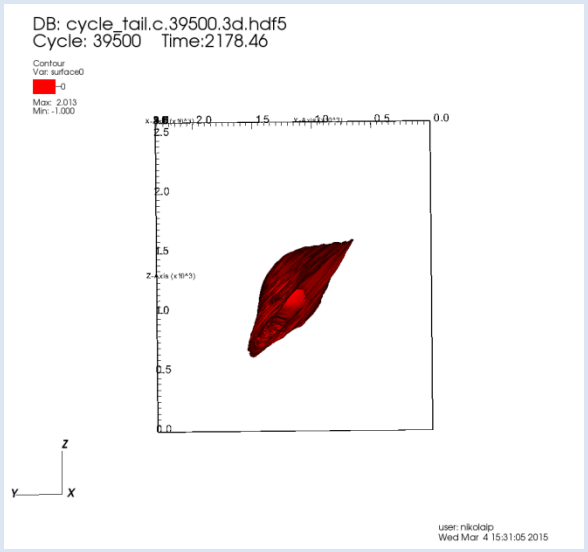

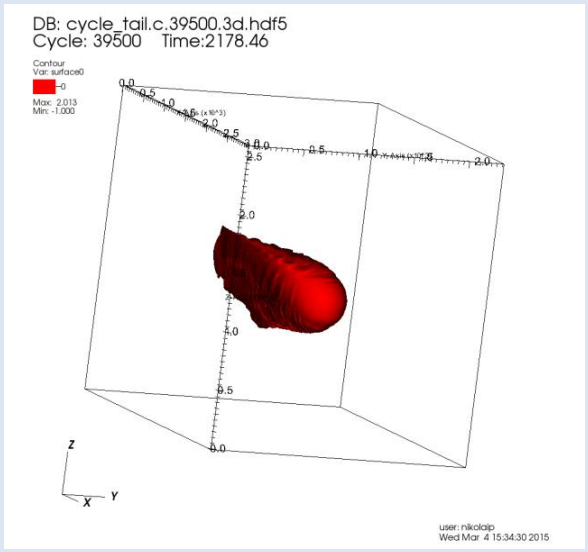

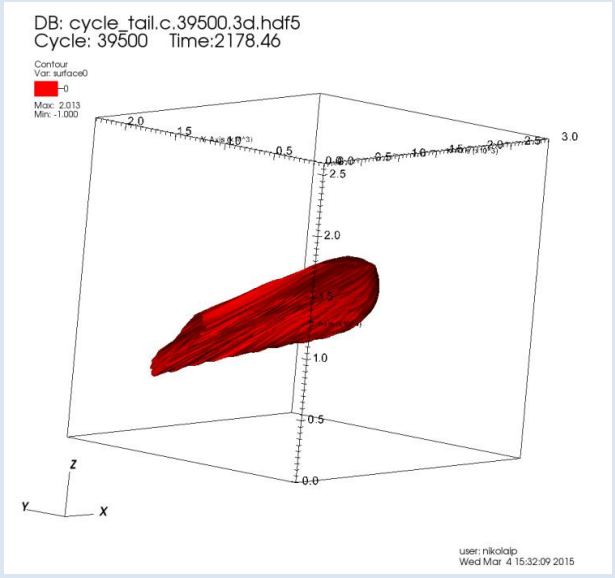

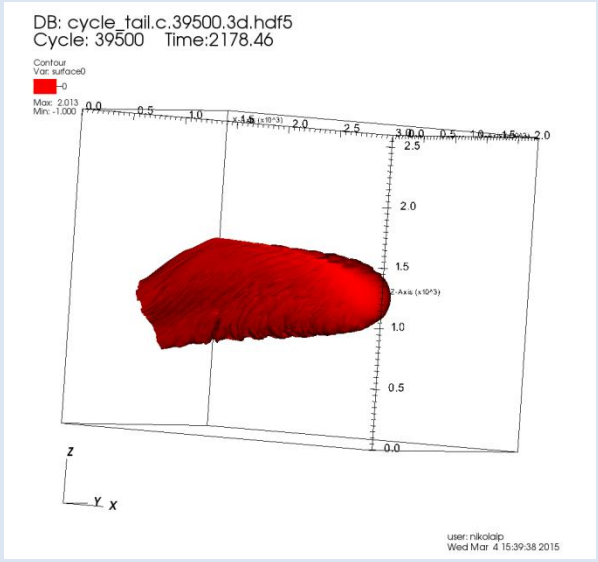

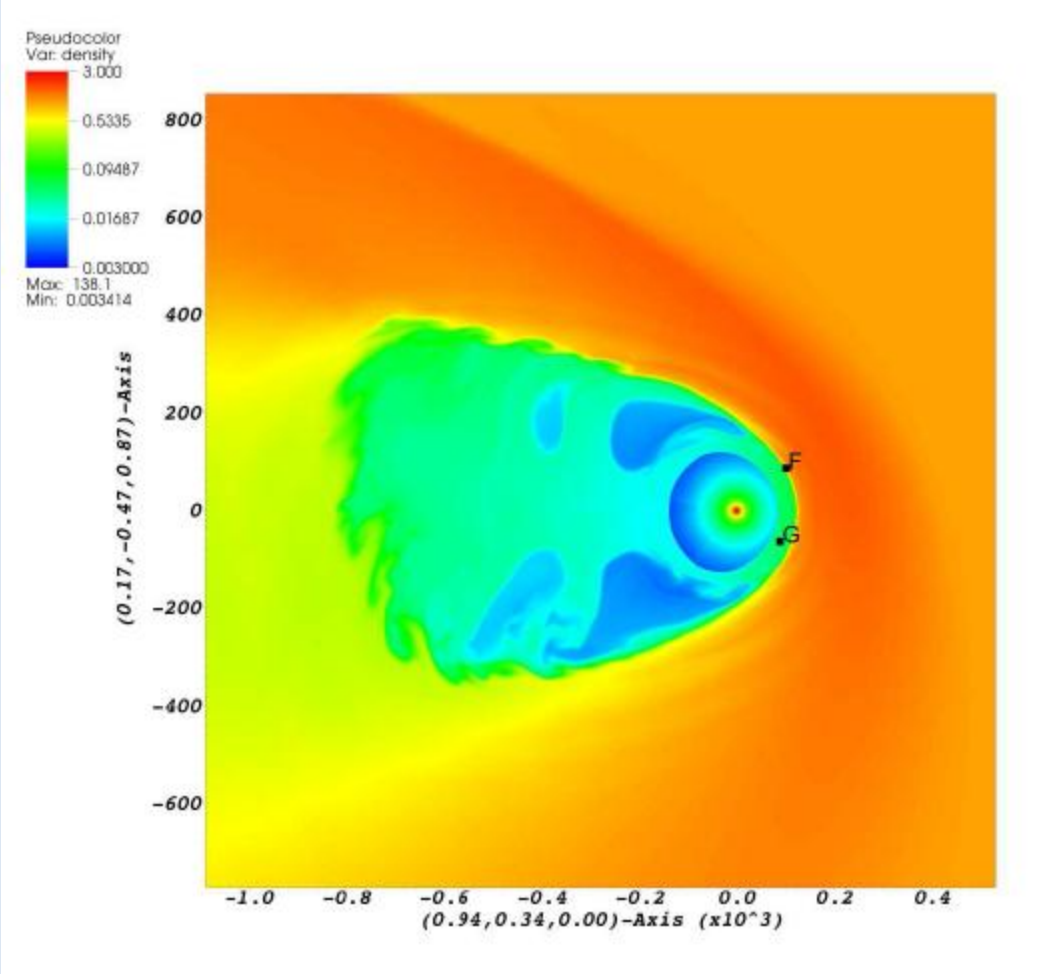

Plasma density in the V1-V2 plane and the spacecraft positions on January 1, 2015. The HP is at 126 AU in the V1 direction and at 128 AU in the V2 direction. With some scaling, V2 will possibly cross the HP in 5 years. I will not bet on 5, because 4 and 6 are also possible.

Conclusions

1. **The combination of SOHO, IBEX, Voyager, and air shower observations provides us with a powerful tool to constraint the properties of the LISM.**
2. **Combining macro- and micro-scales is essential for the explanation and interpretation of observational data.**